University Kasdi Merbah Ouargla
Faculty of Hydrocarbons, Renewable Energies, and Earth and Universe Sciences
Department of Earth and Universe Sciences

Dissertation

ACADEMIC MASTER

Domain: Earth Sciences
Field: Geology

Specialty: Geology of Sedimentary Basins

Presented by:

Rihab ROUAINE

THEME:

Petrology, mineralogy, and geochemistry of phosphorites from southern Djebel Onk (case study of the Tarfaya–Kef Essenoun section, Tébessa)

Publicly defended on

The 19/06/2025

IN FRONT OF

Mr. Mohamed Salah BELKSIER	Prof.	UKM-Ouargla	President
Mr. Rabah KECHICHED	Prof.	UKM-Ouargla	Supervisor
Ms. Safia SAOULI	PhD candidate	UKM-Ouargla	Co-Supervisor
Mr. Abdellatif REMITA	MAA	UKM-Ouargla	Examiner

Academic year 2024/2025

DEDICATION

" يَرْفَعِ اللَّهُ الَّذِينَ آمَنُوا مِنْكُمْ وَالَّذِينَ أُوتُوا الْعِلْمَ دَرَجَاتٍ وَاللَّهُ بِمَا تَعْمَلُونَ خَبِيرٌ "

سورة المجادلة الآية 11

To my dearest **family**...

My beloved **mom** and **dad**, whose love knows no limits, your sacrifices, your prayers, and constant support have been the cornerstone of my life and this academic trip.

Dad **Laid. R** instilled in me the determination to achieve my goals.

Mom **Sabah SAADAOUI** taught me the true meaning of patience.

My cherished sisters and brothers, **Ferdous**, **El Khansa**, **Mohamed Yousri**, **Mohamed Loai**, **Sabaa**, **Mohamed Abdul Monaim**, **Tamaddor**, **Mohamed Ouis** (**Fadi**), and **Mohamed Abdul Badie** (**Fahed**). Thank you for your encouragement, prayers, and the strength you give me every day. Each of you holds a special place in my heart, and your belief in me has been a constant source of motivation.

I also extend my deepest gratitude to my co-supervisor, **Safia SAOULI**, whose insightful guidance, patience, and generous support have been invaluable throughout this academic pursuit. I am truly grateful for your mentorship.

And to my friend, **Khadra**. Thank you for being by my side.

This dissertation is a tribute to your love, support, and inspiration. I share this achievement with you all. with love and gratitude.

Rihab ROUAINE

ACKNOWLEDGMENTS

ACKNOWLEDGMENTS

First, I would like to express my deepest gratitude to my dissertation supervisor, **Pr. Rabah KECHICHED**. You helped me improve my skills and better focus my research topic. Thank you for inspiring me with hope, determination, and courage to complete this thesis. Thank you for sharing your extensive experience and knowledge of phosphate with me. Working alongside you has been enriching, both scientifically and personally. Thank you for your patience and encouragement, and above all for your ethics and great devotion in helping me complete this thesis.

I am so thankful to **Ms. Safia SAOULI**, as co-supervisor, for guiding me during the preparation of this thesis.

I would like to express my sincere thanks to the members of the jury who did me the honor of reviewing and evaluating this thesis: President **Dr. BELKSIER Mohamed Salah** of Kasdi Merbah University in Ouargla and examiner **Dr. REMITA Abdel Latif** of Kasdi Merbah University in Ouargla. I thank you for your availability and for your critiques, which have enriched this work.

I would also like to thank **Mr. Omar GADJA**, the Sahara Geology Laboratory Engineer at the Ouargla Scientific Research Center, and **Pr. Messaoud HACINI**, Director of the Sahara Geology Laboratory, for their invaluable assistance with X-ray analysis (XRD).

I am also deeply grateful to my family and friends, who are always have asked me, “when are you going to present your thesis?” Although it could be confusing at times during moments of doubt, they served as a steady reminder to stay focused on my goal and never give up.

TABLE OF CONTENTS

TABLE OF CONTENTS

CHAPTER I: GENERALITIES

CHAPTER II: GEOGRAPHY, REGIONAL AND LOCAL GEOLOGY

CHAPTER III: PETROGRAPHIC, MINERALOGICAL, AND GRAIN SIZE OFPHOSPHATE

CHAPTER IV: GEOCHEMICAL CHARACTERIZATIONOF PHOSPHATES

LIST OF FIGURES

LIST OF FIGURES

LIST OF TABLES

LIST OF TABLES

ABSTRACT

ABSTRACT

Phosphate deposits in the Tarfaya region, on the southern flank of the Djebel Onk basin (northeastern Algeria), belong to a Maastrichtian–Quaternary sedimentary sequence and are subdivided into three sub-layers (basal, main, and upper) based on lithological, mineralogical, and geochemical features. A multidisciplinary study involving petrography, XRD, and grain size analysis reveals that phosphate grains mainly consist of pellets and coprolites in a matrix of carbonate fluorapatite, dolomite, and quartz, with minor glauconite and fish teeth. Grain size data indicate predominantly fine, well-sorted sands, especially in the main sub-layer, the most economically significant. Geochemical profiles highlight vertical variability: the basal layer shows moderate P_2O_5 (22.13–24.52%), low MgO (avg = 1.99%), and CO_2 (avg = 8.47%); the main layer is more heterogeneous (P_2O_5: 19.61–31.07%, MgO: 0.76–3.79%, CO_2: 4.32–14.11%); and the upper layer presents intermediate values (P_2O_5: 26.19%, MgO: 2.66%, CO_2: 8.97%). Strong negative correlations between P_2O_5 and both MgO ($r = -0.66$) and CO_2 ($r = -0.68$), along with a positive correlation between MgO and CO_2 ($r = 0.98$), suggest mineral segregation between phosphate and dolomitic-carbonate phases, reflecting the influence of depositional conditions on phosphate quality.

Keywords: phosphate, Tarfaya, Djebel Onk, fluorapatite, coprolites, pellets, glauconites, grain size, XRD, petrography, Paleocene-Eocene, P_2O_5, MgO, CO_2, geochemical.

الملخص

تنتمي رواسب الفوسفات في منطقة طرفاية، على الجانب الجنوبي لحوض جبل أونك (شمال شرق الجزائر)، إلى تسلسل رسوبي من العصر الماستريشي-الرباعي، وتنقسم إلى ثلاث طبقات فرعية (القاعدية، والرئيسية، والعليا) بناءً على الخصائص الصخرية والمعدنية والجيوكيميائية. تكشف دراسة متعددة التخصصات تشمل البتروغرافيا والتحليل بالانتشار الضوئي للأشعة السينية وتحليل حجم الحبيبات أن حبيبات الفوسفات تتكون أساسًا من كريات وكوبريتات في مصفوفة من فلوراباتيت الكربونات والدولوميت والكوارتز، مع وجود كميات قليلة من الجلوكونيت وأسنان الأسماك. تشير بيانات حجم الحبيبات إلى وجود رمال ناعمة ومصنفة جيدًا بشكل أساسي، خاصة في الطبقة الفرعية الرئيسية، وهي الأكثر أهمية من الناحية الاقتصادية. تسلط الملامح الجيوكيميائية الضوء على التباين الرأسي: تظهر الطبقة القاعدية نسبة معتدلة من P_2O_5 (22.13-24.52٪) ونسبة منخفضة من MgO ، و CO_2 (متوسط 1.99٪)، ؛ أما الطبقة الرئيسية فهي أكثر تباينًا (P_2O_5: 19.61-31.07٪، MgO: 0.76-3.79٪، CO_2: 4.32-8.47٪) تشير الارتباطات .(P_2O_5: 26.19٪، MgO: 2.66٪، CO_2: 8.97٪) ؛ والطبقة العليا تظهر قيمًا متوسطة(14.11٪ r) CO_2 و MgO ، إلى جانب الارتباط الإيجابي بين(CO_2 (r = -0.68 و MgO (r = -0.66) و P_2O_5 السلبية القوية بين ، إلى وجود فصل معدني بين مراحل الفوسفات والكربونات الدولوميتية، مما يعكس تأثير ظروف الترسيب على (0.98 = جودة الفوسفات.

الكلمات المفتاحية: الفوسفات، طرفاية، جبل أونك، الفلوراباتيت، الكوبرولیت، الكريات، الجلوكونيت، حجم الحبيبات، ، البتروغرافيا، العصر الباليوسيني-الإيوسيني، الجيوكيمياء XRD،CO_2، MgO، P_2O_5.

RÉSUMÉ

Les gisements de phosphate de la région de Tarfaya, sur le flanc sud du bassin du Djebel Onk (nord-est de l'Algérie), appartiennent à une séquence sédimentaire maastrichtienne-quaternaire et sont subdivisés en trois sous-couches (basale, principale et supérieure) d'après leurs caractéristiques lithologiques, minéralogiques et géochimiques. Une étude pluridisciplinaire comprenant la pétrographie, la XRD et l'analyse de la taille des grains révèle que les grains de phosphate consistent principalement en pastilles et en coprolithes dans une matrice de fluorapatite carbonatée, de dolomite et de quartz, avec un peu de glauconite et de dents de poisson. Les données relatives à la taille des grains indiquent la prédominance de sables fins et bien triés, en particulier dans la sous-couche principale, la plus importante d'un point de vue économique. Les profils géochimiques mettent en évidence la variabilité verticale : la couche basale présente une teneur modérée en P_2O_5 (22,13-24,52 %), une faible teneur en MgO (moyenne = 1,99 %) et en CO_2 (moyenne = 8,47 %); la couche principale est plus hétérogène (P_2O_5 : 19,61-31,07 %, MgO : 0,76-3,79 %, CO_2 : 4,32-14,11 %); et la couche supérieure présente des valeurs intermédiaires (P_2O_5 : 26,19 %, MgO : 2,66 %, CO_2 : 8,97 %). De fortes corrélations négatives entre P_2O_5 et MgO ($r = -0,66$) et CO_2 ($r = -0,68$), ainsi qu'une corrélation positive entre MgO et CO_2 ($r = 0,98$), suggèrent une ségrégation minérale entre le phosphate et les phases dolomitiques-carbonatées, reflétant l'influence des conditions de dépôt sur la qualité du phosphate.

Mots-clés : phosphate, Tarfaya, Djebel Onk, fluorapatite, coprolithes, pellets, glauconites, taille des grains, DRX, pétrographie, Paléocène-Eocène, P_2O_5, MgO, CO_2, géochimie.

GENERAL INTRODUCTION

GENERAL INTRODUCTION

Phosphate rocks are among the most strategically vital natural resources due to their central role in global agriculture and industry. Phosphorus, a non-substitutable element, is an essential nutrient for all living organisms and plays a fundamental role in key biological processes, including energy transfer, genetic inheritance, and cellular development. As such, phosphate-bearing deposits have long been the focus of scientific, economic, and strategic interest, particularly in regions with significant geological endowments such as North Africa.

Algeria holds a prominent position among phosphate-rich countries, primarily due to the extensive deposits found within the Tébessa region, in the northeastern part of the country. One of the most significant formations in this area is the Djebel Onk phosphate basin, which contains some of the largest reserves in North Africa. The region's phosphate occurrences are predominantly sedimentary in origin, deposited in a complex and dynamic geological setting that reflects a long history of marine transgressions, tectonic activity, and sedimentary processes. Among these, the Kef Essenoun-Tarfaya region represents a particularly important zone for detailed scientific investigation due to its accessible stratigraphy, varied lithofacies, and economic importance.

This study focuses on the petrological, mineralogical, grain size, and geochemical characterization of the phosphate layer within the Djebel Onk South, specifically in the Kef Essenoun -Tarfaya deposit. The primary objective is to explore the formation processes, mineral associations, textural features, and chemical compositions that define these phosphatic sequences. The study also aims to shed light on the depositional environments and diagenetic processes that have influenced the genesis and post-depositional evolution of the phosphate beds.

To achieve this, a multidisciplinary approach has been adopted, combining detailed field observations, stratigraphic profiling, petrographic microscopy, X-ray diffraction (XRD) analysis, and geochemical analysis. This integrated methodology not only allows for an accurate identification of primary and secondary phosphate minerals (primarily carbonate fluorapatite) but also provides critical insights into associated gangue materials, including dolomite, quartz, and clay. Moreover, the study addresses grain size distributions that help conclude sedimentary dynamics, energy regimes, and post-depositional reworking.

A key aspect of this research is the comparative analysis of different phosphate sub-layers (basal, main, and upper) in terms of their mineralogical content and geochemical signatures, particularly with respect to their P_2O_5 and MgO concentrations. This stratified analysis is critical for identifying the most economically viable horizons and for understanding lateral and vertical facies variations across the deposit.

In addition to its scientific objectives, this dissertation also contributes to the broader context of resource management and sustainable development in Algeria. As global demand for phosphates continues to grow (driven by population growth, food security concerns, and new industrial applications), the need to optimize the exploitation of existing reserves becomes increasingly urgent. Understanding the detailed geology of these deposits is a foundational step in achieving more efficient, economically sound, and environmentally responsible mining practices.

In this context, the Djebel Onk south region, particularly the Kef Essenoun- Tarfaya deposit, offers a valuable case study that encapsulates the broader geological, economic, and environmental themes associated with phosphate mining in North Africa. The results of this study will thus be of interest not only to geologists and mineralogists but also to policymakers, environmental planners, and industry stakeholders involved in phosphate exploration and exploitation.

CHAPTER I

G E N E R A L I T I E S

CHAPTER I

G E N E R A L I T I E S

1. General overview on phosphates

Phosphorus is one of the 19 elements strictly indispensable to the growth and development of all living beings, whether microbial, vegetal, or animal. There is no other element in the periodic table that can replace P in three processes specific to life: reproduction, energy transfers, and respiratory mechanisms.

This element is widely distributed in nature. It is found in soils, oceans, and wastewater, either as mineral salts or in complex combinations with nitrogenous soil matter.

The term natural phosphates are used to describe all ores containing minerals with the P-O bond. They are used primarily as fertilizers, with the main source being sedimentary rocks with over 80 % apatite, most often in the form of apatite fluor hydroxyl [$Ca_5(PO_4)_3$ (F, Cl, $OH)^-$]. Since the 20th century, many phosphate deposits have been recognized and identified around the world, notably in the USA and North Africa.

1.1. General definition

Phosphate ores are characterized by the presence of the radical $(PO_4)^2$. The terms “phosphorite” and “phosphatite” are used with the following meanings (Slansky, 1980):

- Phosphorite It's a sedimentary rock composed mainly of phosphate minerals. Phosphorite can be clayey, siliceous, or carbonate, depending on the gangue.
- A phosphatite is a rock containing, by weight, at least 50% phosphate minerals; its lower limit has been set at 18 % P_2O_5.

Under these conditions, the terms phosphorite or phosphatite can only be used for rocks with P_2O_5 contents of 18 % or more.

1.2 Types of phosphate deposits

1.2.1. Sedimentary deposits

This category of phosphates accounts for more than 85 % of world production. It is widespread and can be found in a wide variety of geological layers. The most interesting platform deposits are associated with synclinal structures and are developed in arid climates.

The sedimentary ore facies are of three types: pseudo-oolithic granular facies, nodules, and organic debris (coprolites and phosphatized fossils) (Fig. 1).

1.2.2. Deposits of magmatic or igneous origin

Deposits of igneous origin are currently the least numerous, providing 12 % of the world's phosphate production. These deposits contain up to 37 % P_2O_5. They are found in very ancient ground, where they can form layers dozens of meters thick. In this type of deposit, the phosphate is in the form of well-crystallized apatite.

1.2.3. Guanos deposits

They represent the smallest resources but are far from negligible. The most important deposits come from the seabird guanos, which contains around 4 % P_2O_5. These organisms react with the rock that supports them. When the rock is limestone, calcium phosphate is formed. The island of Nauru (Pacific Ocean) is a deposit of the guanos type (Slansky, 1980).

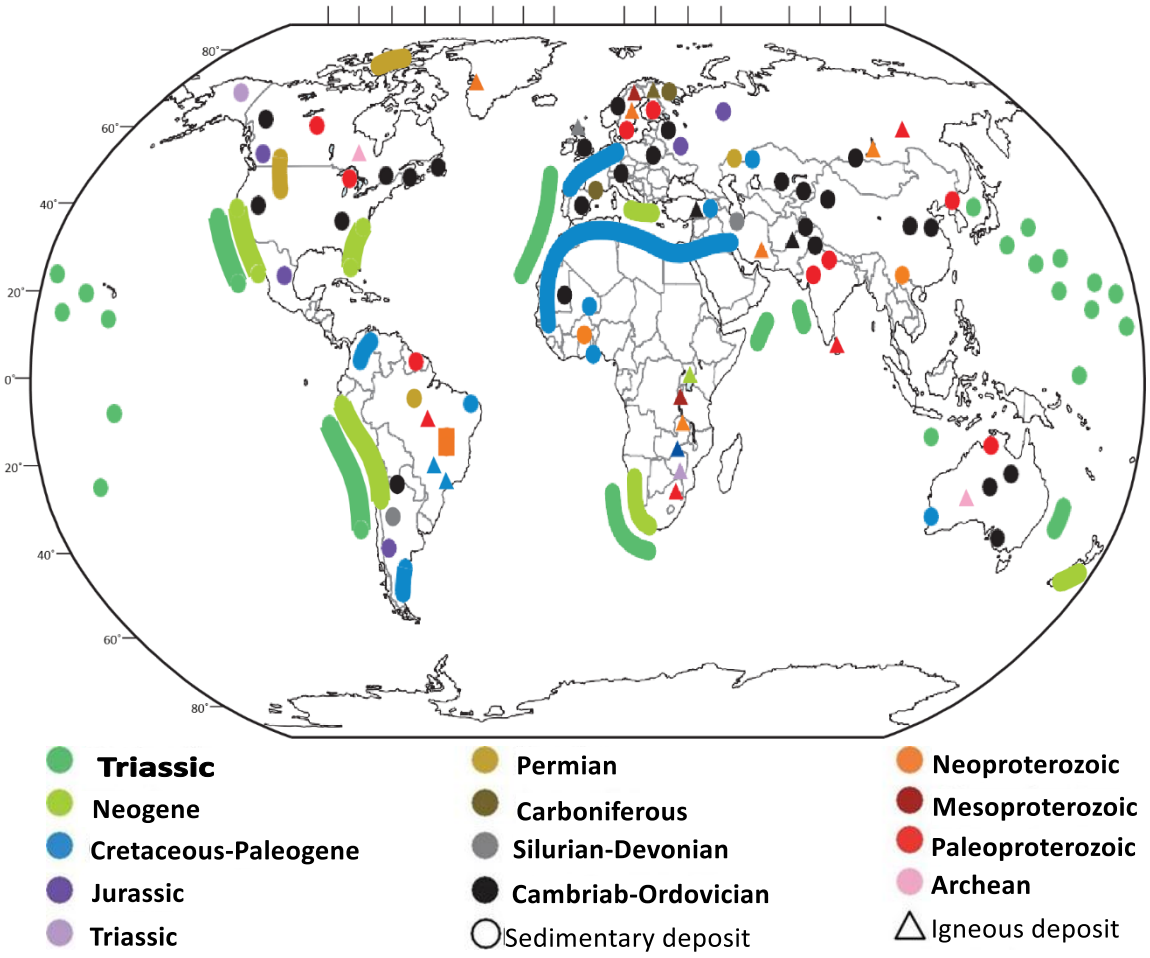

Fig.1: Known igneous and sedimentary phosphates with respective ages. Compiled from (Cook, 1986; Glenn et al, 1994; Notholt et al, 1980).

1.3. Formation of sedimentary phosphate deposits

The set of processes controlling the authigenic precipitation of phosphate minerals, principally francolite, which is a fluorapatite carbonate, is termed phosphogenesis (Föllmi et al; 1993; Jarvis et al; 1994). Phosphogenesis implies biochemical processes (Glenn; Riggs and Föllmi, 1994; Jarvis et al, 1994; Krajewski et al, 1994), which can occur in a wide range of sedimentary environments, from deep basins to anoxic marginal basins (Filippelli, 2011) (Fig. 2).

Most sedimentary phosphate ores are formed by the rise of phosphorus-rich upwelling currents to shallow shelves, where it is extracted from the ocean surface by phytoplankton and converted to apatite by the accumulation of mud rich in organic matter (Glenn et al, 1994; Jarvis et al, 1994). This phenomenon gives rise to fine primary phosphates; sediments conserved in their initial state without undergoing transport or reworking. It is generally low in P_2O_5 (Trappe, 1998; Föllmi, 1996, 2016).

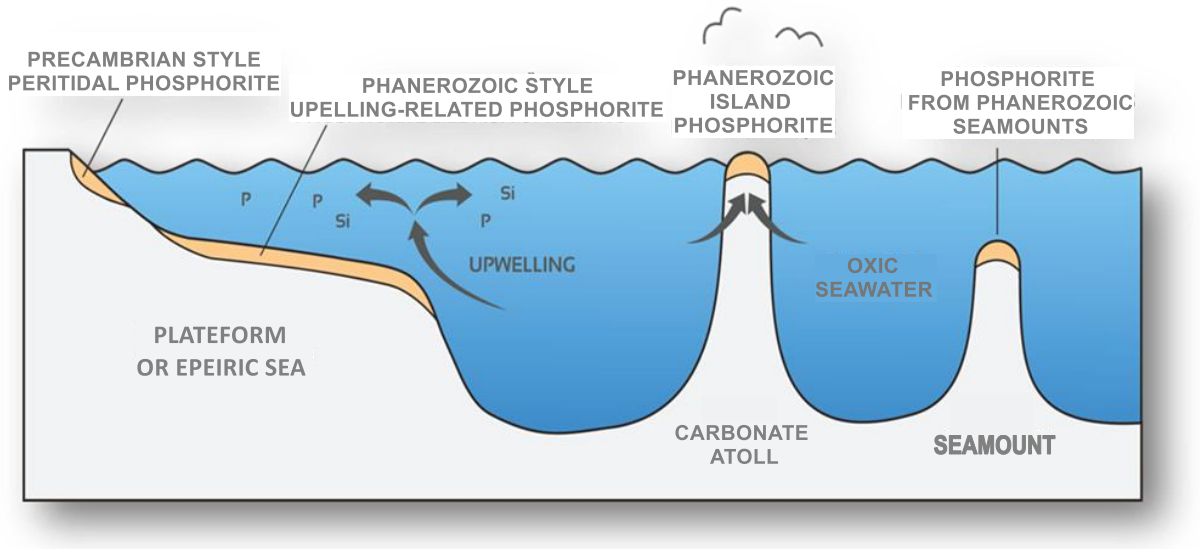

Fig.2: Deposition environments for sedimentary phosphates Majorass phosphate deposits are accumulated on marine platforms and beneath epicontinental seas (Pufahl and Groat, 2017).

Phosphogenesis alone cannot lead to phosphate-rich sediments without the intervention of post-phosphogenesis agents that facilitate ore accumulation, concentration, and enrichment (Baturin, 1982) (Fig. 3).

These agents are mainly those of hydrodynamics that affect primary phosphates, and, through transport and reworking, typically granular facies are formed (Glenn et al, 1994; Pufahl and Grimm, 2003; Soudry et al, 2013; Pufahl and Groat, 2017). The latter are of economic interest due to their high P_2O_5 content.

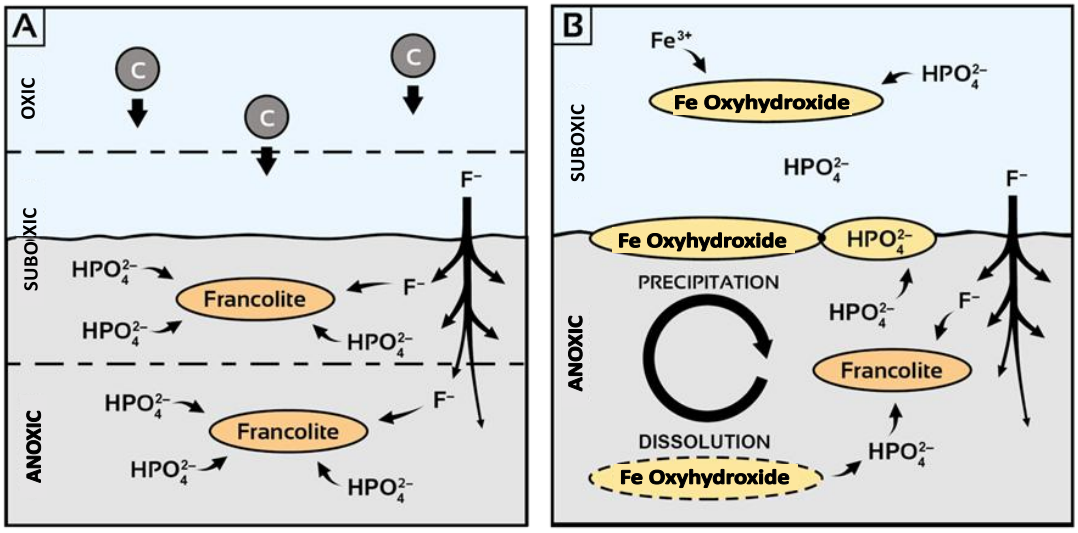

Fig.3: Phosphatogenesis process, figure from (El Bamiki et al., 2021).

(A): Environment with upwellings where microbial degradation of organic matter.

(B): Role of iron oxyhydroxides in pumping phosphorus and maintaining high concentrations of this element that will allow francolite precipitation in environments without upwellings (Pufahl and Groat, 2017).

C: In the sediment, the concentration of dissolved phosphate in the interstitial water increases, provoking the precipitation of francolite. This precipitation is limited at depth by the diffusion of seawater derived F-.

1.4. Phosphate mineralogy

Natural phosphates are minerals formed by the association of metal ions with the phosphate ion $(PO_4)^{3-}$. They comprise over 200 mineralogical species (Fig. 4).

A link has been established between the mineralogy of phosphate constituents in rocks and sedimentary ores. Based on the raw composition of the ores and the mineral species they contain, Mc Clellan, in 1969, classified phosphate rocks into three families: calcium phosphates such as apatitic minerals and the much less common alumino-calcitic or aluminous phosphates such as crandallite, or iron-aluminum phosphates grouped together under the name barren dite. Other secondary minerals from certain phosphate deposits are also reported in sedimentary deposits, such as rare-earth and uranium phosphates. However, the most abundant phosphate minerals belong to the apatite family.

- **Apatites**

Apatites are calcium phosphates also containing fluorine, chlorine, and hydroxyl substitutions. In the organic world, apatite plays a fundamental role as a mineral component of bones and teeth. It is also important in paleontology. Indeed, the fossilization of bones in certain sediments can take place through the partial or total substitution of organic bone molecules by fine apatite crystals. Apatites belong to the hexagonal system and are characterized by the general formula $M_5(XO_4)_3Y$, where M is a divalent alkaline-earth cation, $(XO)_4$ and Y are multivalent and monovalent anions, respectively.

Natural apatites are the products of a considerable number of substitutions.

The most common apatite is fluorapatite ($Ca_5(PO_4)^{3-}F$), in which F can be partially replaced by OH or Cl to form hydroxylapatite and chlorapatite respectively. However, the most marked substitution in apatites is that of $(PO_4)^{3-}$ by $(CO_3)^{2-}$. The introduction of additional F- ions helps preserve the crystal's electrical neutrality. On the other hand, a frequent substitution in apatites also concerns Ca^{2+} ions by Na+ and Mg^{2+} have shown that this substitution has a direct relationship with that of $(PO_4)^{3-}$ by $(CO_3)^{2-}$.

The apatite network allows numerous other substitutions, generally more discreet than the previous ones. Calcium can be substituted by Mn, Sr, Mg, rare earths, Na, K, H_2O, H_3O^+, Cu, Sn, Pb, U... The $(PO_4)^{3-}$ ion can also be substituted by $(SO_4)^{2-}$, $(SiO_4)^{4-}$, $(H_4O_4)^{4-}$, $(AsO_4)^{3-}$ and $(CrO_4)^{2-}$. $(SO_4)^{2-}$ ions can be substituted for $(PO_4)^{3-}$ in ways comparable to $(CO_3)^{2-}$ in some cases and significantly less so in others.

1.4.1. Gangue minerals

The gangue minerals associated with phosphate elements in phosphate rocks are very numerous. They are mainly:

- Sedimentary ores, mainly quartz, calcite, dolomite, ankerite, siderite, alkali feldspars, clay minerals (montmorillonite, attapulgite, illite, sepiolite, chlorite, and kaolinite), gypsum, salt, goethite, limonite, pyrite, organic matter, etc.
- Ores from igneous and alkaline rocks, represented by nepheline, quartz, and the minerals of pegmatites, proxenets, carbonates, ijolites.... etc.

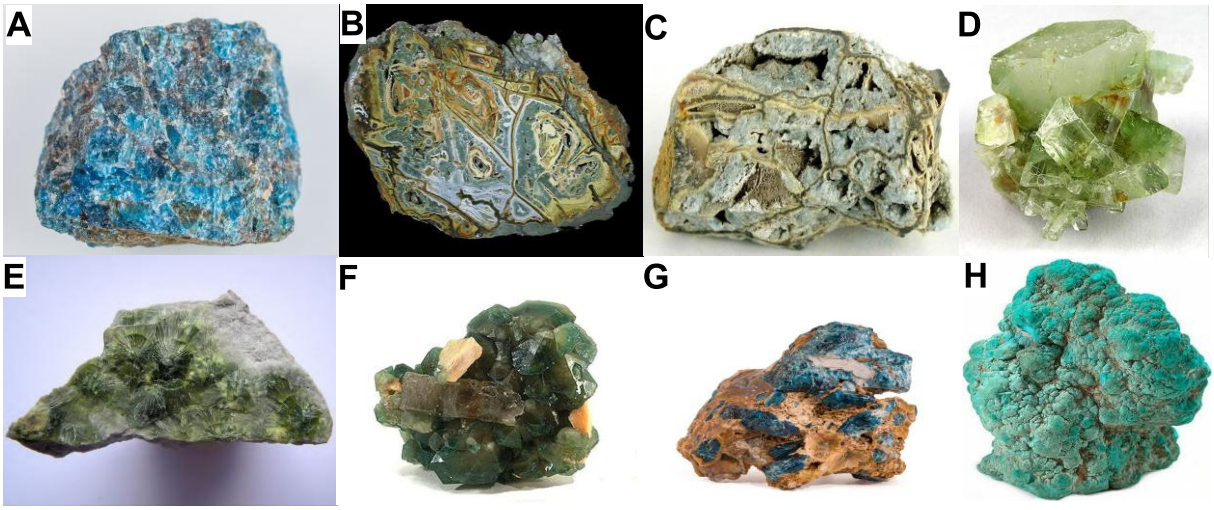

Fig. 4: The different minerals that make up phosphates

(https://commons.m.wikimedia.org/w/index.php#/search).

1.5. Phosphate morphology

The non-phosphate fraction of the rock is divided into an endo-gangue within the phosphate-bearing elements and an exo-gangue outside them. This distinction is important in mining geology, as in phosphate ore treatment, the endo-gangue is evidently more difficult to eliminate than the exo-gangue (for example, pelphospharenite with pyritic endo-gangue and organic-rich clay exo-gangue).

The exo-gangue corresponds to the entire sterile part of the ore, made up of the binding phase and non-phosphate figurative elements. It is extremely variable in quantity, nature, and aspect from one ore to another. It mainly comprises :

- **Carbonates:** very frequent in phosphate deposits. Calcite, dolomite, ankerite…
- **Silica:** clastic quartz is frequent in the exo-gangue of exploited phosphatites, flint, ... etc.
- **Silicates:** there are several clay minerals in the exo-gangue: kaolinite, montmorillonite, attapulgite, glauconite... etc.

The fractions mentioned in the next section are the most common in phosphatite exo-gangues, which may also contain iron in the form of sulfides, carbonates, or oxides; gypsum; and sometimes barite.

In the absence of excessive secondary oxidation, exo-gangue is often rich in organic matter, especially when it is clayey.

In the nomenclature of phosphatites, exo-gangue is as important as the size of phosphate grains. It is characterized by its mineral composition, the size of its grains or crystals, and its relative abundance in the rock.

The endo-gangue is made up of all the non-apatitic fractions within the phosphate elements. The most common minerals are

- **Quartz:** can be common in the endo-gangue of phosphate pellets. A pellet may contain several grains of quartz, but more often than not, it contains only one, around which the apatite is distributed in one or more layers.
- **Organic matter:** this is the constant endo-gangue of pellets that have not undergone too much secondary oxidation. It is distributed in any way, in the center, on the periphery, or in concentric layers.

1.6. Phosphate chemistry

Phosphate ores are defined according to their P_2O_5 content or in terms of percentage of tricalcium phosphate (TPL or BPL: Bone Phosphate of Lime), which is really the basic phosphate product (1 TPL = 2.185 P_2O_5).

Geochemical studies carried out on a series of phosphate ores by different authors have evidenced the association of chemical elements with phosphate mineral phases such as clays, carbonates, apatites, silica..... etc.

Different dosages of the elements making up these mineralogical phases (P_2O_5, MgO, CaO, SiO_2, Al_2O_3, Fe2O3, TiO_2, Na_2O, K_2O, etc.) have made it possible to determine the distribution of the elements and their link with the mineral phases.

- Major elements are associated with the main mineralogical phases present (apatite, clay, carbonates, silica). Loss in ignition is mainly related to clays and carbonates.
- Minor and trace elements are only associated with clay and phosphate phases.
- A series of elements characterizing clays are: Ba, Cr, Cs, Cu, Ga, Mo, Nb, Ni, Pb, Rb, Sb, Sn, Sc, Sr, V, Zn and Zr.
- A series of elements characterizing apatite are: Ce, Dy, Er, Gd, Ho, La, Lu, Nd, Pr, Sm, Tb, Th, Tm, U, Y, Yb and Sr.

1.7. Phosphate distribution

1.7.1. Phosphates in the world

The world's leading phosphate-producing countries are Morocco, the United States, Russia, and China. They account for over 80 % of world production, expressed in millions of tons (Mt) of ore in place.

1.7.2. Phosphates in Algeria

Algeria has a significant potential phosphate reserve. The country's main phosphate concentrations are represented by the two major phosphate sedimentation domains of Eocene age:

- The Hodna Mountains in northern Algeria and the Nememchas-Tébessa Mountains in southeastern Algeria.
- The Hodna Mountains include the Mzaita, Bordj-Redir, and Maadid deposits.

These deposits vary considerably in content (12 to 23 % P_2O_5), with reserves of just over 10 million tons at Mzaita, where the phosphate is particularly rich in silica (25 % SiO_2 on average). The phosphate layers at Bordj Redir, which reach 25 % P_2O_5 over a thickness of 2.5 meters, are penalized by abnormally high iron and alumina contents (nearly 7 %).

In all three formations, the phosphate layers contain sterile intercalations that compromise their exploitation.

The Dyr, Kouif, and Djebel Onk deposits make up the phosphate ensemble of the Nememchas-Tébessa mountains, which is present in the most extensive outcrops:

- **Dyr deposit:** located some twenty kilometers northeast of Tébessa, has important P_2O_5 contents (up to 31 %), but the deposit's reserves are less important.
- **The Kouif deposit** is located 23 kilometers northeast of Tébessa, in a synclinal elliptical basin parallel to the Dyr axis and extending into Tunisia. The five layers exploited, which are up to 3 meters thick, have grades of around 30 % P_2O_5. With reserves virtually exhausted, declining profitability and economic constraints

- **The Djebel Onk formation** is Algeria's largest phosphate deposit, both in terms of reserves and ease of access and exploitation.

1.7.3. History of phosphates in the Tébessa region

In 1873, Philippe Thomas discovered Algerian-Tunisian phosphate layers near Rass-El-Ajoun, in southwest Tunisia, and in 1893, the Dj-Dyr quarry was discovered as well as the Kouif level in the same period. The Société Nationale de la Recherche Minière (SON.AR.EM) took over minings of the El Kouif deposit. Then, in the 1906-1907 period, M. Joleau discovered the Djebel Onk deposit (at Djemi-Djema, south of Djebel Onk); airborne radiometric surveys were effectuated over the Djebel Onk basin in the 1961-1963 period. Exploitation of the Djebel Onk deposits began in February 1965 at Djemi-Djema by the « Société de Djebel Onk ». Following the development of the quarry, interest in the geology of Djebel Onk grew, and the Enterprise de Recherche Minières (EREM) was commissioned by the Société Nationale du Fer et des Phosphates (FERPHOS) to research and evaluate phosphate resources, which mined Djebel Onk phosphate between 1985 and 1987. In 2016, a study performed on rare earth elements (REEs) by Kechiched, et al, (2016) in the southern basin (Dj-Onk deposit), highlighted that REE contents are between 174.41 and 906.39 ppm (∑REE on average = 623.01 ppm), while the northern phosphorites have lower ∑REE contents (from 125.45 to 472.44 ppm , on average 265.57 ppm) ; Recently, (the work of Kechiched, et al, in 2017), identified the rare earth element contents of various phosphate sites in northern and southern Tébessa on a sedimentological, gîtological, and geochemical level.

1.8. Phosphate economies

1.8.1. Phosphate production

Phosphates are classified 11th out of the 53 natural substances marketed in the world, representing a value of $3-4 billion a year.

Global phosphate reserves are estimated at 70 billion metric tons based on USGS data (Jasinski, 2020). Morocco alone holds around 72 % of reserves. China holds around 4.6 % of reserves, mostly in the Neoproterozoic formation. In the United States, which has 1.5 % of the world's reserves, phosphate production comes mainly from deposits of Middle Miocene age in Florida and North Carolina (Jasinski, 2020).

China is the world's leading phosphate producer (110,000 Mt), followed by Morocco (36,000 Mt) and the USA (23,000 Mt) (Jasinski, 2020). Phosphate prices have started to rise in recent years, making it possible to exploit deposits with low P_2O_5 contents (<20 %) and to use new technologies. (Fig. 5).

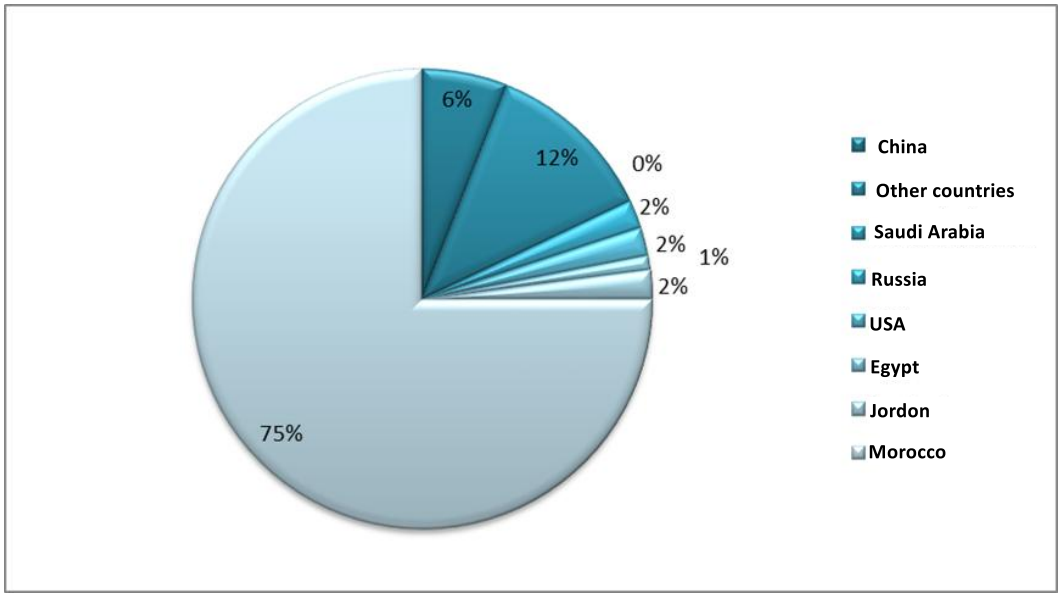

Fig.5: World phosphate rock reserves. (Data from USGS, 2020).

1.8.2. Use of phosphates

Most of the world's phosphate production (95 %) is destined for agricultural use in the form of fertilizers (Cissé and Mrabet, 2004). In addition to its classic use in the fertilizer industry, phosphorus is used in a number of other industrial fields: the food industry, detergents, textiles, plastics and wood treatment, and metallurgy for cleaning and protection or anti-corrosion coating. In the chemical and petroleum industries, phosphorus is used to manufacture particularly active intermediate derivatives (sulfides, chlorides, oxides, etc.). New developments in the phosphate industry are to be found in the cutting-edge medical domain of biomaterials. The development of apatite bioceramics or apatite-loaded polymers as materials for bone replacement or dental implants is currently under study. The dispersing power of phosphates has led to their use in multiple industries to separate or combine finely dispersed liquids and solids.

1.9. Environmental aspects of phosphates

Natural phosphates contain metal cations that can be recovered as by-products (U, TR, V, Ti... etc.) (Aly Monir and Mohammed Nabawia, 1999; Cherniak, 2000; Rakovan and Reeder, 1996)

or eliminated because they represent an environmental hazard (U, Cd, Mo, Se, As... etc.) resulting from the use of phosphate fertilizers (Baioumy, 2005; Baturin and Kochenov, 2001; Beji Sassi et al, 1999).

Cadmium levels in European soil have become one of the EEC's main preoccupations in recent years. It has been estimated that 30-60 % of cadmium in crops comes from the atmosphere and 40-70% from the soil. One source of cadmium in the soil is phosphate fertilizers. With the current rate of use of these fertilizers, especially in industrialized countries, there is an accumulation of cadmium in the soil.

Along with nitrate, phosphorus is a major responsible for eutrophication. Another environmental problem is that phosphogypsum heaps produced by industrial fertilizer production contain radioactive elements. For this reason, studies have been carried out to recover and decontaminate phosphates, with the aim of recovering certain elements, such as uranium, or eliminating certain toxic or nuisance elements, such as cadmium and heavy metals.

Conclusion

In this chapter, we provided an overview of phosphate deposits, their types, and modes of formation, with a particular focus on their mineralogical and chemical characteristics. We explored the major types of deposits (sedimentary, igneous, and guano) and examined the processes behind their formation, including the role of phosphogenesis and post-depositional changes.

The global distribution of phosphate resources was discussed, with special attention given to Algeria's significant reserves, notably in the Tébessa region, which holds strategic importance due to its rich and accessible phosphate layers. We also reviewed the historical context and development of phosphate exploitation in Algeria, highlighting key discoveries and production activities.

Moreover, the chapter addressed the economic importance of phosphates, emphasizing their dominant use in agriculture as fertilizers and their growing applications in industry, medicine, and environmental technologies. This multifaceted perspective on phosphates underscores their value as a critical natural resource.

CHAPTER II

GEOGRAPHY, REGIONAL AND LOCAL GEOLOGY

CHAPTER II

GEOGRAPHY, REGIONAL AND LOCAL GEOLOGY

INTRODUCTION

This chapter delves into the regional and local geological framework of the Djebel Onk area, a region of critical economic and scientific importance in northeastern Algeria. Positioned near the Algerian-Tunisian border, the study area encompasses several key phosphate-bearing deposits, including Kef Essenoun and Tarfaya, which lie within the broader Djebel Onk mining district. The chapter outlines the geographical, stratigraphic, structural, and tectonic settings that define this zone, with a focus on its rich phosphatic formations spanning from the Upper Cretaceous to the Quaternary. Through detailed stratigraphic analysis and tectonic interpretations, the chapter aims to contextualize the geological evolution of the region and establish a foundation for understanding the distribution, composition, and economic potential of the phosphate resources. This geologic insight is essential for effective exploration and sustainable exploitation of the mineral wealth that characterizes the Djebel Onk area.

1. Geographical situation of the study area

1.1.Geographical situation of Djebel Onk

The Djebel el Onk region is located 100 km south of the wilaya of Tébessa and 20 km from the Algerian-Tunisian border, on the road between Tébessa and El Oued (Fig.8). This region forms the geographical limit between the Hauts Plateaux of Constantine and the Saharan domain. Topographically, the Djebel Onk massif forms a 20 km-long limestone ensemble, culminating at Djebel Tarfaya at 1198 m altitude. The lowest altitudes at the foot of Djebel Onk are around 635 m.

The Djebel Onk region is subdivided into 5 mining sectors:

- Djemi-Djema deposit.
- Kef Essenoun and Tarfaya deposits.
- Djebel Onk Nord deposit.
- Oued Betita deposit.

- Bled El Hadba deposit.

The Kef Essenoun deposit, currently quarried by SOMIPHOS, is only 4 km from the town of Bir El Ater.

1.1.1. Geographical situation of Kef Essenoun

The Kef Essenoun deposit is part of the Djebel Onk mining basin (Tébessa South). It is located in the extension of the rare southern fall of the Djebel Onk antiformal flexure and, more precisely, at the foot of the Djebel de Kef Essenoun. The plateau forms a gentle southwesterly slope. Topographic heights range between 720 m in the southwest and 810 m in the northeast.

1.1.2. Geographical situation of Tarfaya

Djebel Tarfaya is located in northeastern Algeria, on the southern flank of the Djebel Onk within the Tébessa region. Geographically positioned near the Kef Essenoun area, it lies approximately between longitudes 6°25′E and 6°35′E and close to latitude 39°00′N. This region is notable for its stratigraphic sequence spanning the Maastrichtian to the Eocene, featuring limestone, marl, gypsum, and thick phosphate-rich layers. Djebel Tarfaya is geologically significant due to its lateral facies equivalence and variable thickness in phosphate units, making it an essential reference for lithostratigraphic correlations and phosphate exploration within the Djebel Onk mining district.

2. Regional geology

The region of Tébessa in Algeria is one of the most important regions for economic development, as it contains important natural resources, namely phosphate. In this region, phosphates are located at a wilaya gold deposits of El-Kouif, Djebel Dyr and Tazbant and in the south where the deposits of Djebel Onk near the town of Bir-El-Ater.

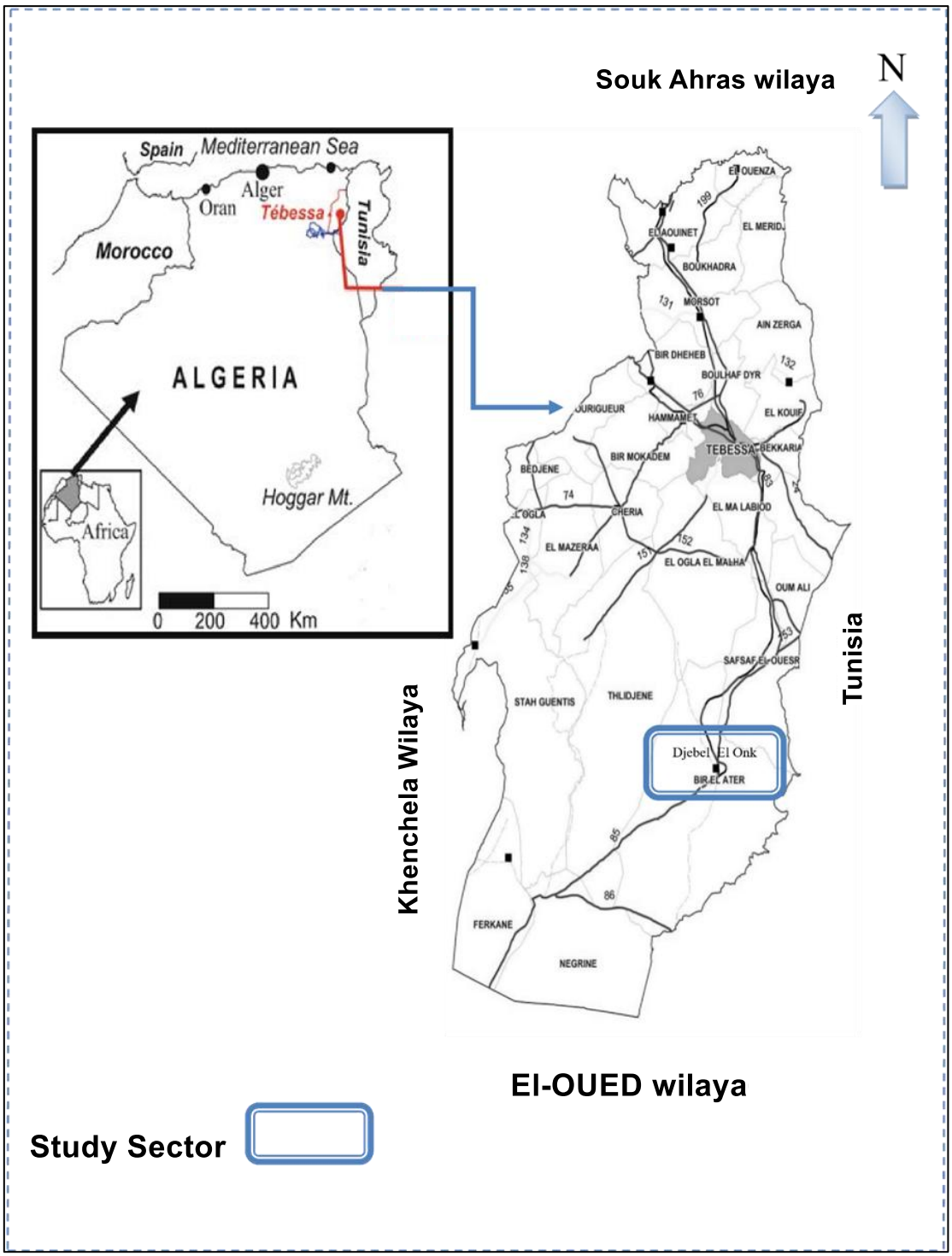

Fig.6: Geographical location of the Djebel Onk region.

2.1.Stratigraphy of Djebel Onk

The stratigraphy of the Djebel Onk region was 1st studied by (Visse 1952). The sedimentary series outcropping is expressed by a stratigraphic succession from Upper Cretaceous (Maastrichtian) to Middle Eocene (Lutetian), surmounted by a continental sandy-clay series dated to the Miocene and Quaternary. (Fig. 7)

2.1.1. Cretaceous

The Cretaceous corresponds to the most ancient sediments at the heart of the very rugged tectonic Djebel Onk anticline. Only Maastrichtian deposits are exposed.

- **Maastrichtian**

Sediments of this age, at the heart of Djebel Onk, are represented by flinty limestones and marl intercalations (5 to 10 m). In their upper part, they represent a tapped, rubefied surface that is easy to identify in the topography.

2.1.2. Paleogene

These are marine sediments represented by limestones, phosphates and gypsum. In the region, the Paleogene reaches thicknesses of 350 m. Lithological variations and the rests of organisms have made it possible to make the following stratigraphic subdivisions:

- **Danian**

It differs from the Cretaceous, and is conventionally adopted from the Maastrichtian limestone-contact clay-marl series. This lithological difference is presented by a subdivision into two distinct series, where we note the separation between the Upper Danian and the Lower Danian. The total thickness of the Danian is around 100 m.

- ***Lower Danian*:** represented by shaly marly clays, dark grey to greenish-brown in color, intercalated by hard, irregular marls. The ensemble is traversed by gypsum filons of different orientations.
- ***Upper Danian*:** formed by very fine, hard white limestones, often with conchoidal fractures, with intercalations of soft, clayey and schistose marls. In the upper part of the Danian, a characteristic 1 to 2 m thick bed of beige lumachelle limestone is topped by white platelet marl. The first thin layers (10 to 30cm) of phosphate marl appear in this stage.

- **Selandian**

This stage is marked by the presence of a series of limestones, detritic limestones, lumachelle limestones with intercalations of marl and dolomite. These sediments are characterized by an absence or small quantity of flint. Oysters are abundant, in gray to black beds.

- **Thanetian**

This is the horizon bearing the mineralization and is visible on the flank of the Djebel Onk anticline, with a thickness of 72 m. It is subdivided into two:

- ***Lower Thanetian:*** Characterized by marly schists irregularly interspersed with limestone. These schists are dark gray to black in color. At the base are gastropod conglomerates, thin phosphate layers and a series of intercalated marls with characteristic faunas rich in organic matter. In the upper part of the Lower Thanetian, phosphate intercalations up to 2 m thick, very rich in organic matter, are topped by limestones and marls with large gastropods. The thickness varies from 30 to 40 m.
- ***Upper Thanetian*****:** begins with a dolomitic gastropod level, underlying a phosphate layer 30 m thick on average at Djebel Onk and Bled El Hadba, which diminishes until it disappears to the north, west and south of this deposit, generally ending with a lumachellic level. The limit between the Thanetian and the Ypresian is marked by a change from phosphate facies to marly limestones with a thickness of 0 to 50m.

2.1.3. Eocene

- **Ypresian:** rests directly on Thanetian deposits and outcrops in the Djemi-Djema quarry and north of Djebel Onk. It is 32 m thick. Note:

  - ***Lower Ypresian*****:** represented at the base by conglomerates marking the limit with the Thanetian and underlain by a layer of alternating limestone, marl, dolomite, and the phosphate layer. Thin layers of flint are present in the limestone. The average thickness of the Lower Ypresian is 30 m maximum.
  - ***Upper Ypresian*****:** alternating limestone, dolomitic limestone and marl; 2 to 3 m thick.

- **Lower Lutetian:** characterized by a significant decrease in limestone. These are replaced by soft white marl. Note the presence of quartz geodes and flint nodules. The Lower Lutetian is 40 to 50 m thick.

- **Upper Lutetian:** This is an evaporitic series. It is composed of gypsum, greenish clay, green phosphate clay, and limestone. Also of note is the presence of a 10 m thick layer of green phosphate clay and limestone at the base and a layer of green clay with an intercalated layer of gypsum at the top. It is 65 m thick, and its characteristic fauna includes Ostréa Multicostata and Cardia Placunoides.

2.1.4. Miocene

It is composed of terrigenous rocks, conglomerates, clays, sands, and schists. It is subdivided into three concordant formations superimposed one on top of the other:

- **Lower Miocene:** mainly conglomerates, sand, and thin layers of siliceous clay. Its thickness reaches 200 m.

- **Middle Miocene:** represented mainly by clays, sometimes schists, with interlayers of fine and medium-grained sands. It is 250 m thick.

- **Upper Miocene:** This is sandy-clay-conglomeratic facies. It is 350 m thick.

2.1.5. Quaternary

Quaternary deposits are widespread. It is mainly represented by slope scree, eolian sandy deposits, gravels, boulders, alluvial (colluvial, delluvial), and fluvial deposits.

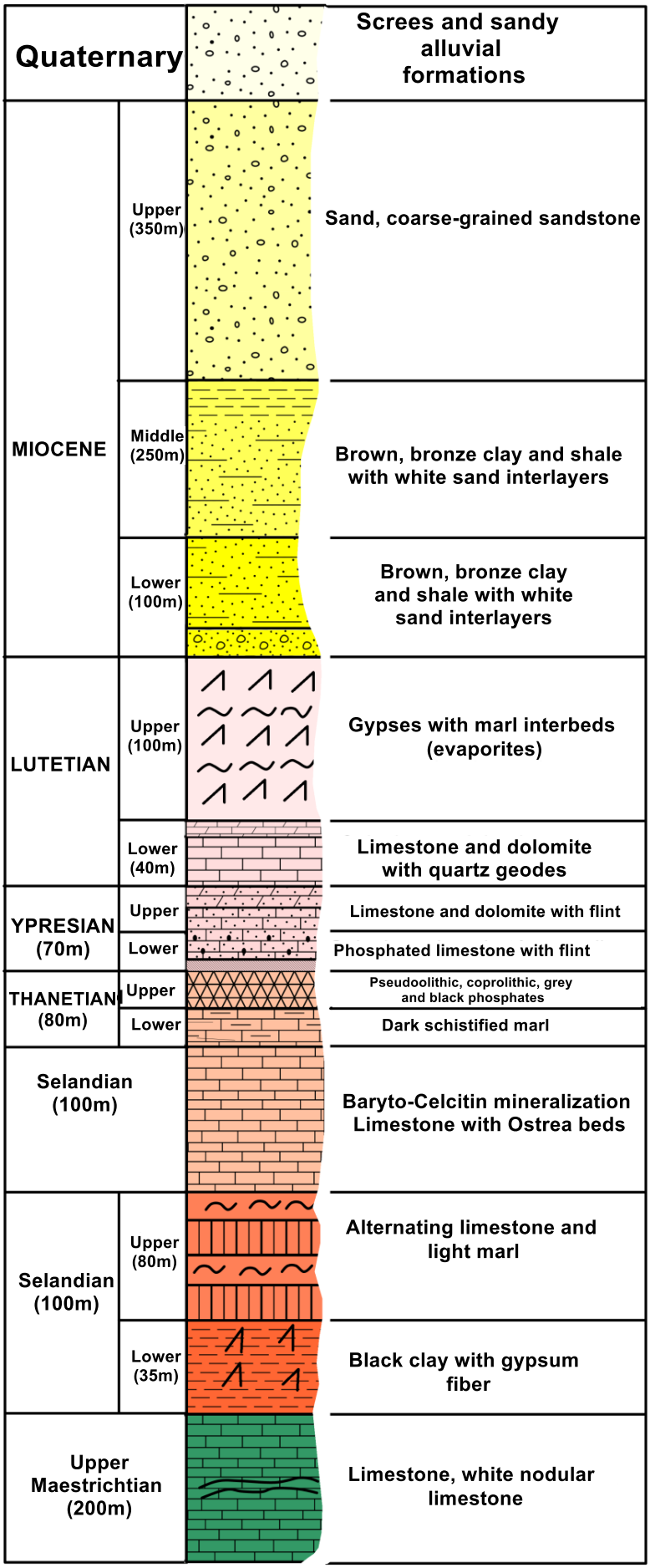

Fig.7: Stratigraphic column from the Djebel Onk region, eastern Algeria (Based on Cielensky and Benchernine, 1987).

2.2. Regional tectonics

2.2.1. Geological structure

The Djebel Onk region and the Tunisian Atlas belong to the oriental edge of the Saharan Atlas. Structurally, the Djebel Onk anticline is located on the limit of the South-Atlasic flexure (Ranchin, 1963), which represents a confrontation zone between the active Atlasic domain and the stable Saharan platform. More precisely, they belong to the northern branch of the flexure, which curves in an E-W direction (Fig. 8). The Upper Cretaceous to Eocene formations of the Djebel Onk-Gafsa-Métlaoui basin are structured by a series of asymmetrical anticlines and synclines (Fig. 8), generally faulted on their flanks. The disposition of the anticlinal and synclinal structures is linked to dextral shear movements along the Gafsa fault, oriented N120° E.

The main structure in the Bir El Ater region is the central Upper Cretaceous Djebel Onk anticline, extending for around 20 kilometers along a N70°N axis and around 3 kilometers wide. Described by Visse (1951) as a post-Pliocene anticline, this highly asymmetrical anticline has a gently sloping northern flank of less than 10° supporting the northern Djebel Onk deposit, and its southern flank is very steep, sometimes vertical or even upside down (Fig. 8).

At a distance of 770 m to the south of Djebel Onk, which culminates in Djebel Tarfaya at 1198 m, a small, low-lying anticline of Djebel Djemi-Djema, 883 m high, stands out. This anticline has a 70° NE axis, with a Lower Thanetian marl core and Upper Thanetian phosphate core. The Djebel Onk and Djebel Djemi-Djema anticlinal structures are separated by a lowering, about 1 km wide, interpreted by Ranchin (1963) as collapsed synclinal troughs filled by Miocene and Quaternary detrital deposits. The Kef Essenoun monoclinic deposit is expected in the southwestern extension of this synformal structure and its northern flank (Fig. 9).

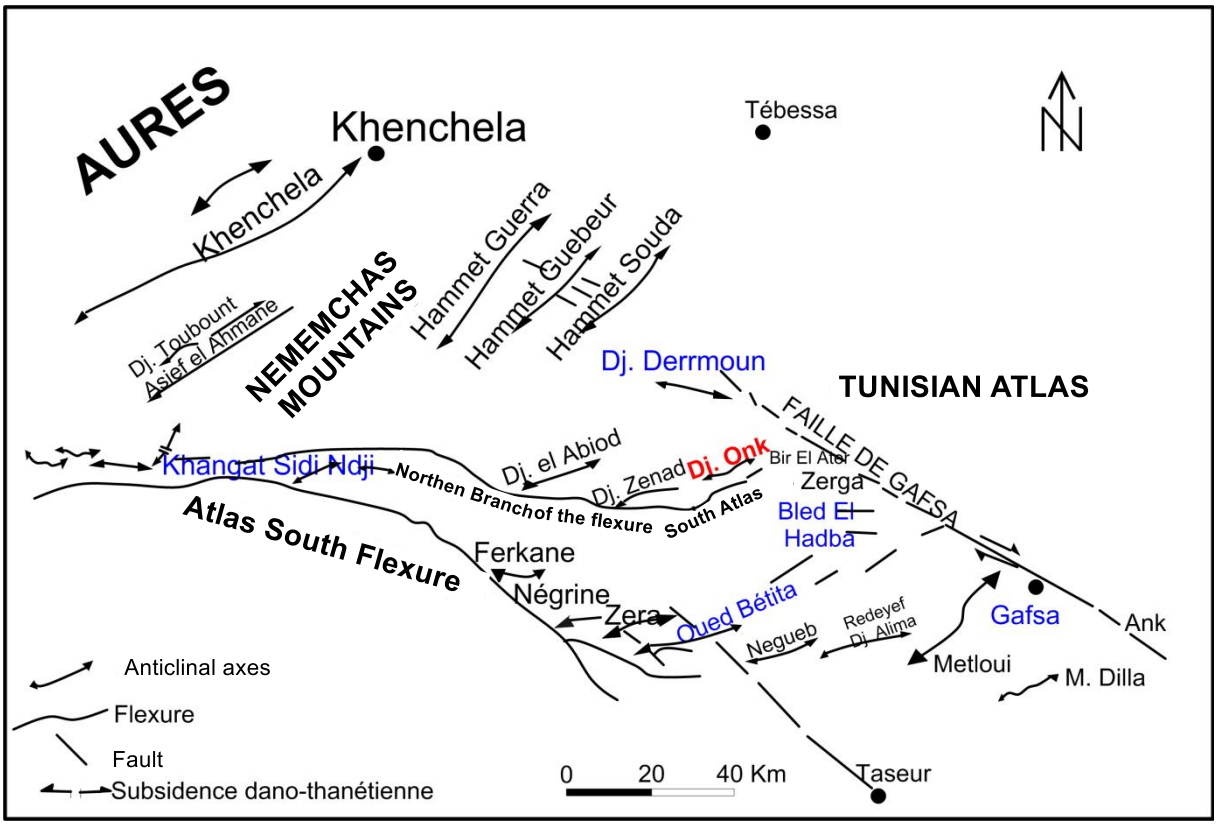

Fig.8: Structural map of the Djebel Onk region within the Gafsa-Métlaoui-Onk basin (Aissaoui, 1984).

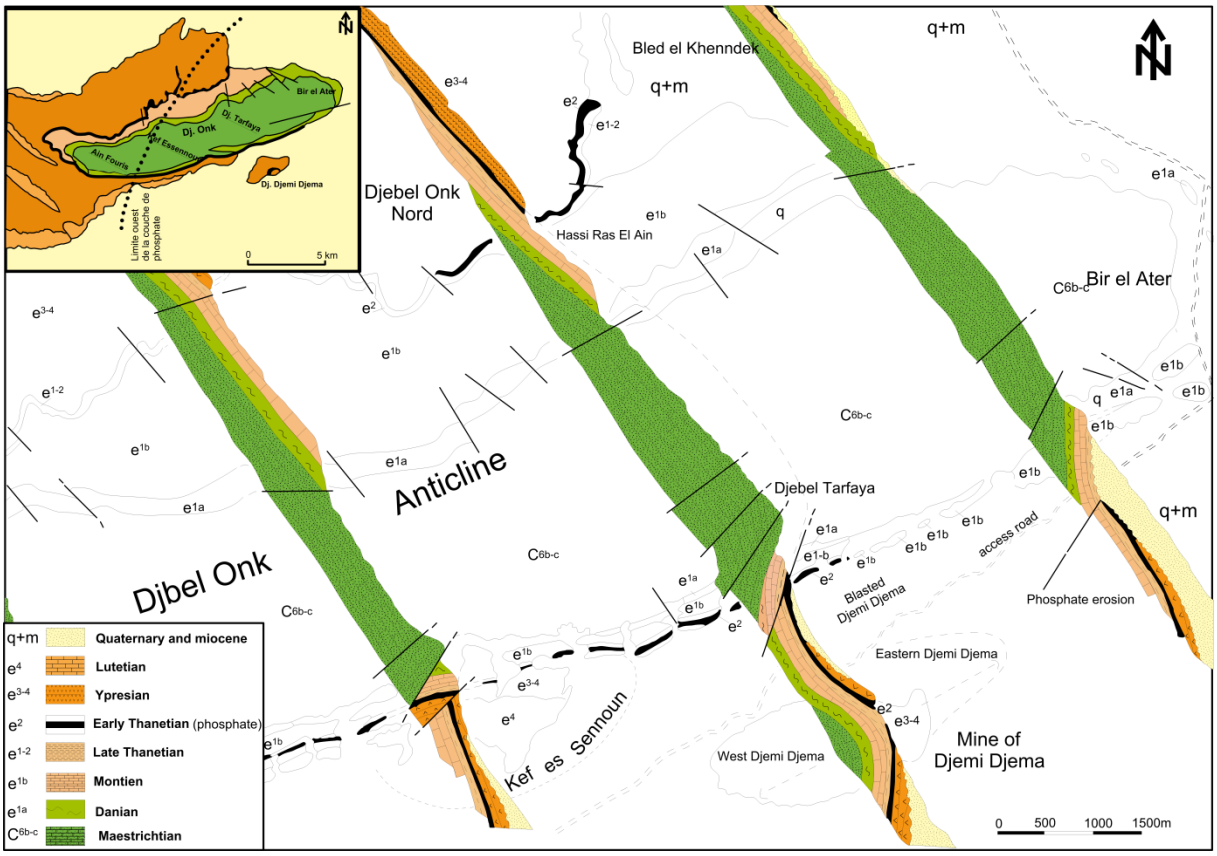

Fig.9: Stratigraphic and structural sections of the northern and southern flanks of Jebel Onk (Cielensky and Benchernine, 1987).

2.2.2. Chronology of deformation phases

The current structure is the result of three deformation phases (In Prian and Cortiel, 1993):

- **Syn-sedimentary tectonics (Paleocene-Eocene):** determined by sedimentary platform structural instability and NW-SE compression, concomitant with Paleogene deposition, represented by syn-sedimentary undulations and faults. These early tectonics induced sedimentary gaps in the Paleocene-Eocene series, leading to the construction of paleogeographic systems of shallows and furrows that controlled phosphate deposition. These early deformations are thought to be associated with diapir uplift (Triassic), particularly in the Paleocene-Eocene.
- **Post-Middle Eocene, Tardi-Miocene tectonics:** coincides with the emergence of the series in the Upper Lutetian. It represents a major stage in the folding of the Aures and extensive lateral deformation (N120° to 140°E faulting), inducing the start of structuring of the Upper Cretaceous-Eocene series into small horsts and grabens, and extends along N70°E in the Dj-Onk and Djemi-Djema areas, which will be affected by late Miocene differential erosion. These folds mainly predate the Miocene sand deposits. This tectonic phase contributed to the formation of the Djebel Onk anticline (Mezghache and Hani, 2000).
- **Tradi-Miocene Post-Burdigalian to Paleocene-Pleistocene tectonics:**

This is the main phase of folding in the Tunisian Atlas. The folding of the Upper Cretaceous-Paleocene-Eocene and Miocene series into large antiform and synform structures is replayed in horsts and grabens in the earlier structures. On the southern inverted flanks, it forms an immense fold (mega-fold) of Jebel Onk and Djemi-Djema. This tectonogenesis is responsible for the current structure of the Jebel Onk region.

2.3. Paleogeography

In Algeria, the end of the Cretaceous is marked by a major period of marine phosphogenesis that proceeded in the Tethys Ocean. Algerian-Tunisian phosphates were deposited around the Kasserine paleoisland (Kechiched et al., 2018) during the Upper Paleocene-Lower Eocene. The Djebel-Onk basin belongs to the occidental part of the Gafsa-Métlaoui-Onk basin (Sassi, 1980). The island of Kasserine, made up of Upper Cretaceous rocks, is bordered by three phosphate basins containing huge quantities of phosphate. The southern basin in our study includes Algeria's world-class commercial phosphate deposits, such as the Djebel Onk mining basins.

These are represented by the Gafsa-Métlaoui-Onk basin located between the Djeffara and Kasserine islands. The Gafsa-Métlaoui basin is located in the transition zone between a strongly faulted and folded zone to the north, the north-central Atlasic domain, and the undeformed Saharan platform to the south (e.g., Zargouni, 1985; Saïd et al., 2011; Garnit et al., 2017). This basin is regularly fed by upwelling currents to the east through the Chemsi Pass and literally with the open ocean of the Tethys to the west (Chaabani, 1995). Sedimentation in the oriental part of the Gafsa-Métlaoui basin occurred under restricted conditions controlled by littoral and lagoonal sedimentation conditions, resulting in rhythmic sedimentation (Sassi, 1974; Chaabani, 1995; Zaïer et al., 1998; Ounis et al., 2008). This led to a diversified sedimentation with cherts, clays, carbonates, marls, gypsum, and phosphates forming several times. These facies vary in age from the Cretaceous to the Quaternary. Phosphate layers appear in the Lower Maastrichtian in the Abiod Formation and then in the Lower Thanetian-Ypresian, which is attributed to the Chouabine Formation. Chabou-Mostefai (1987) used lithological and micro-paleontological data to show the continuity of equivalent succession in the Gafsa-Métlaoui basin in relation to Djebel Onk. The Djebel Onk phosphate deposits are located ~80 km southeast of the town of Tébessa. It is characterized by subsidence and controlled by NW-SE and W-E faults (Visse, 1952). The Djebel Onk basin comprises five distinct phosphate deposits (Djemi-Djema, Djebel Onk Nord, Oued Betita, Bled El Hadba and Kef Essenoun). It comprises thick series deposited from the Upper Cretaceous (Maastrichtian) to the Middle Eocene (Lutetian), in addition to Quaternary continental sediments.

2.4. Mineralogy and petrography of Djebel Onk phosphates

Phosphate ores contain one or more commercially usable phosphate minerals, such as fluorapatite. Consequently, the mineralogy of phosphorus-rich rocks is complex, and there are over 200 known phosphate minerals (Fisher and Jérom, 1973). Phosphate ores are divided into three groups according to their P_2O_5 content: low-grade ores (12-16 % P_2O_5), medium-grade ores (17-25 % P_2O_5) and high-grade ores (26-35 % P_2O_5). Deposits that could be exploited and processed economically to produce around 28-38% P_2O_5 are considered to be commercial phosphate deposits (Sengul et al., 2006). The mineralogical composition of these phosphates shows phosphate matter, in addition to the endo-matrix, which accounts for 5.3 % of phosphate matter; this consists of fluorapatite carbonate (Chabou Mostfai, 1975; Larouci, 1988). The endomatrix may be composed of quartz, illite, organic matter or opal. Three types of exo-matrix (cement) are recorded, including phosphate: the first is carbonate with a predominance of

dolomite, the second clayey, siliceous with glauconite and the third, sulfate with traces of epsomite, which is rare. Dolomite cement dominated and was even limited to the upper and basal parts of the phosphate formation. Mineralogically, the apatitic phosphate of Jebel Onk is a fluorapatite carbonate (Larouci, 1988). Most of the layer consists of dark and light phosphates, with grain sizes ranging from fine (100 µm) to coarse (up to 1 mm).

Phospharenites (25 % of the reserve) are present above dark phosphates in the northern part of the layer (EREM 1987). From base to upper, the phosphate layer is made up of alternating marl-phosphate-dolomite and phosphate dolomite, which is the productive layer. Chemically, the productive layer is remarkable for its high P_2O_5 content and low MgO content, for both types of ores. The average P_2O_5 content ranges from 25 to 27.9 %, for a general average of 26.53 %. MgO contents are constant and low (2 and 3 %) throughout the layer. There are many gangue minerals associated with phosphate elements in phosphate rocks: quartz, calcite, dolomite, ankerite, siderite, feldspars, clays, gypsum and organic matter, among others.

3. Local geology

3.1. Kef Essenoun

3.1.1. Stratigraphy

The stratigraphy of the Kef Essenoun deposit was investigated by exploration work carried out by EREM in 1986 (Cielensky and Benchernine, 1987). Core drill holes were carried out on a 250 m x 300 m grid (Fig. 10). The deepest hole is S-7 (250 m), located to the south-west of the deposit. The shallowest hole is S-25 (76.1 m), located close to the Kef Essenoun outcrop. All drill holes penetrated the phosphate layer right up to the wall, with the exception of survey hole S-14, which intersected only 13.5 m due to a technical accident during drilling. In addition, EREM drilled 22 trenches in the dressant zone, marked Tr22 to Tr44, with a depth of 1 to 2 m, a width of 1 m and a length depending on the thickness of the phosphate layer outcrop.

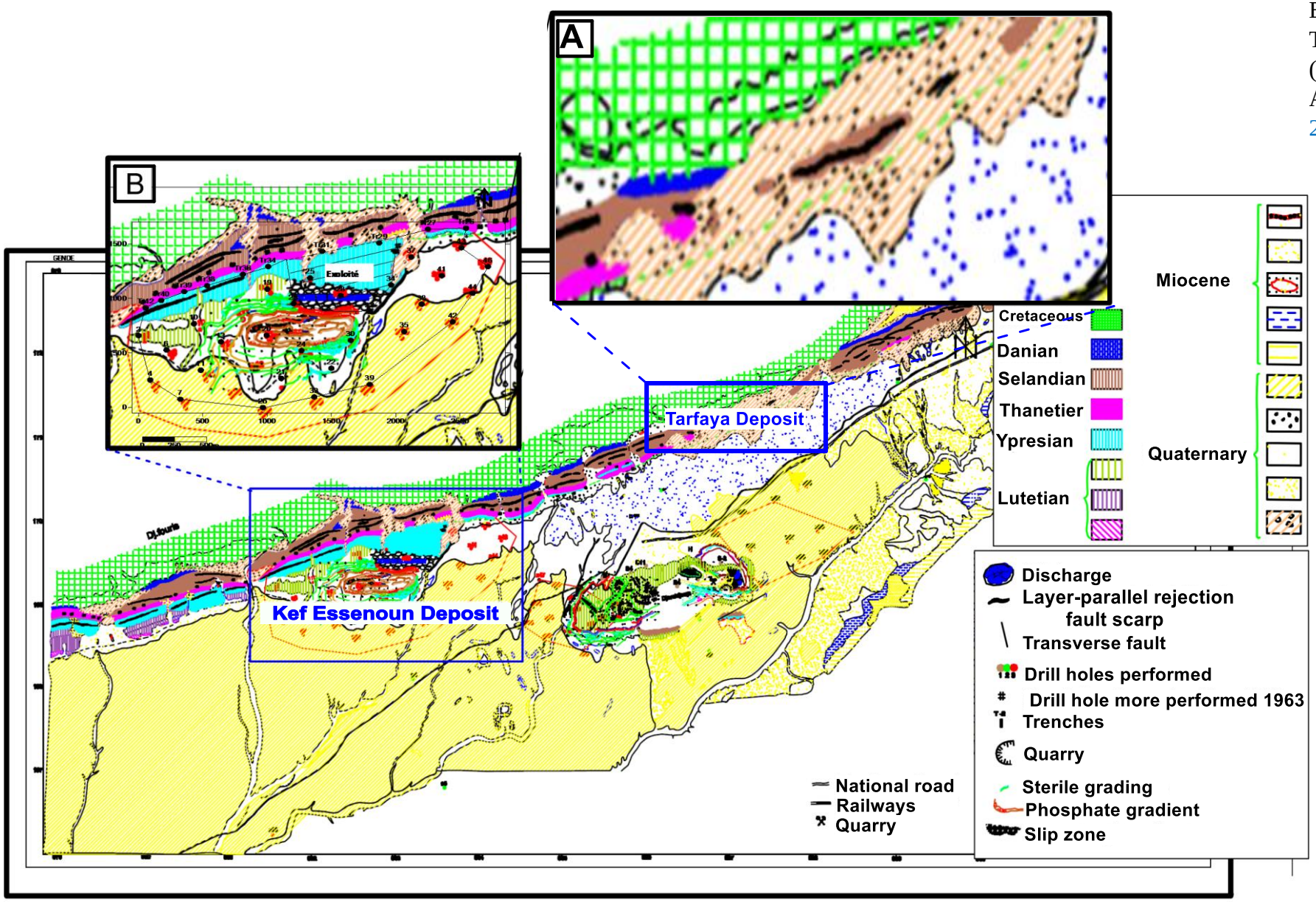

Fig. 10: Location of drill holes and trenches at the Kef Essenoun and Tarfaya deposit (Djebel Onk, eastern Algeria). (Ferhaoui, 2023)

The Djebel Onk stratigraphic series is to be found at Kef Essenoun. The stratigraphy of the Kef Essenoun deposit is simple, and was well defined by Cielensky et al, from 1985 to 1987. It is represented by Cretaceous (Maastrichtian) to Quaternary formations:

- **Cretaceous**

  Maastrichtian: Compact, chalky, sonorous white limestone with inoceramus.

- **Paleocene**

  Paleocene deposits are largely developed in the region. It is subdivided into:

- **Danian**

- ***Lower Danian:*** composed of greenish-gray clay marl interbedded with limestone.
- ***Upper Danian:*** mainly composed of very fine limestones intercalated with clayey marls containing decimetric levels of phosphates.

- **Selandian:** lumachelle limestone with intercalations of marl and dolomite.
- **Thanetian:** the mineralized horizon is well developed and divided into two levels:

- ***Lower Thanetian*****:** represented by a series of dark-gray schitized marls with irregular limestone intercalations. A conglomeratic level with gastropods and thin phosphate layers are found in the lower part. At the upper part, the phosphates are surmounted by limestones and marls with large gastropods.
- ***Upper Thanetian*****:** indicated by the productive layer, represents the main phosphate material deposited on the southern margins of Djebel Onk and is relatively thicker (average ~ 35 m) than the phosphate levels in the northern deposits (Cielensky et al., 1988; Prian and Cortiel, 1993). The Upper Thanetian phosphate layers of the Kef Essenoun deposit, similar to all the deposits of Djebel Onk, are divided into three sub-layers (basal, main and upper sub-layers) according to their characteristic petrological and chemical properties (P_2O_5 and MgO); from base to top we can distinguish (Prian and Cortiel, 1993).

Basal sub-layer: composed of alternating phosphate, marl and dolomite, with an average thickness of 2 m. The transition to the main sub-layer may be marked by a 40 cm dolomite bench. These phosphate ores alternations are thin (0 to 4 m). This alternation has low P_2O_5 contents (13 to 15 %) and high MgO contents (8 to 10 %) (Kechiched et al., 2020).

The main sub-layer: This layer is characterized by phosphates 25 to 30 m thick, weakly to lightly intercalated with centimetric levels of marl-limestone and dolomite. This sub-layer is

mined because it has the highest P_2O_5 content (P_2O_5 is 28 to 30 % by weight) compared with the other sub-layers (Kechiched et al., 2020).

The upper sub-layer: varying in thickness from 1 to 10 m (average = 3 m), it is often dolomitic and sometimes shows flint levels. It is low in P_2O_5 phosphate particles (< 18 %) and high in MgO (6 to 11 %), very hard, well cemented and with abundant matrix material. As a result, P_2O_5 contents are often lower than in the main sub-layer.

- **Eocene**

- **Ypresian:** divided into:

- ***Lower Ypresian:*** Alternating white marly limestones, marls and dolomites containing flint nodules and thin phosphate layers surmounting a conglomeratic level.
- ***Upper Ypresian*****:** Alternating limestones, dolomitized limestones, marls and phosphate marls. The ensemble contains many flint nodules.

- **Lutetian**

- ***Lower Lutetian:*** White marly limestones and chalky marls with flint nodules. Higher up, gypsum substitutes for flint.
- ***Upper Lutetian:*** Formations of this age alternate between light-colored marls and green, sometimes phosphate-bearing clays, with thin banks of limestone and gypsum levels.

- **Miocene:** continental quartz sand formations with clay lenses.
- **Quaternary:** Represented by alluvial formations and slope scree.

3.1.2. Tectonics

The Kef Essenoun deposit is located in the southern extension of the Djebel Onk antiform flexure, whose major structuring is due to post-Miocene tectonics. It is characterized by a simple structure in the form of a regularly dipping monoclinal table at an angle of 5-10° to the south. To the south of the table, a zone of slope rupture can be seen, where the dip of the layers reaches 20°. A series of three major NNW-SSE faults cross the deposit, but do not generate major deformations in the geometry of the phosphate layer. In contrast, in the Kef Essenoun dressant zone, elongated N 75° E, soft and brittle tectonics have led to an abrupt change in the dip of the outcropping phosphate layer, where the dip angle is sub-vertical or steeply inclined to the southeast or southwest.

3.2.Tarfaya

3.2.1. Definition of lithostratigraphic units

Given the main characteristics and lithological variations of the assemblages described in the sections studied, these assemblages have been grouped into formal lithological units: formations, members and reference layers (or horizons), distinguished according to the nature of the dominant rocks:

- Sets 1 to 5 of Djebel Tarfaya thus constitute the clay formation A, itself subdivided into a predominantly clayey lower member I, formed by clay ensembles 1 and 3 separated by the phosphate-bearing marker layer (horizon) 2, and an upper member II formed by the tight clay-limestone alternations and then laches of assemblies 4 and 5.
- Sets 6, 7 and 8 of the Djebel Tarfaya form the Carbonate Formation B, also subdivided into a lower member I and an upper member II. The lower member corresponds to the "Venericardia beaumanti" marker layer and the still clay-rich set 7, while the upper member corresponds to the predominantly lumachellic and bioclastic facies of set 8.

3.3. Study case of Tarfaya

From the bottom to the top, which the layers are tectonically reversed structure (Fig.11). We have:

- The Marls of **Ta1** (Lower Thanetian) date back to the Thanetian age, which corresponds to the early Paleocene, specifically its lower part. These deposits are typically gray to greenish-gray in color, a common hue for marly formations. The texture is fine-grained, friable, and slightly calcareous, with notable clayey components. As a mixture of clay and carbonate, the marls often exhibit a fissile or laminated structure.
- The phosphates in the Upper Thanetian (Late Paleocene) section (from **Ta3** to **Ta7**) exhibit distinct characteristics in color and texture. Typically, beige (a common hue for phosphatic layers) these deposits vary in structure across different layers. The basal sub-layer (**Ta3**) is nodular or granular, likely containing coarser phosphate concretions. The main sub-layer (from **Ta4** to **Ta6**) consists of dense, massive, or bedded phosphate-rich sediment, which may be sandy or peloidal in composition. The upper sub-layer (**Ta7**, Upper part) transitions to a finer-grained texture, possibly incorporating reworked fragments or blending into the overlying strata.
- The limestones of **Ta9** (Lower Ypresian) date back to the Ypresian age of the Early Eocene. They exhibit a light gray to beige coloration, which is typical of shallow marine

carbonates. The texture of these limestones ranges from fine to medium-grained, often appearing as micritic or bioclastic limestone. They are generally well-bedded and notably harder than the underlying phosphate and marl units.

- **Ta2**: Contact between Upper and Lower Thanetian (it's a sedimentary transition within marls/phosphate precursors).
- **Ta8**: Contact between Upper Thanetian (phosphate) and Lower Ypresian (limestone), marking a major stratigraphic shift (Paleocene-Eocene boundary).

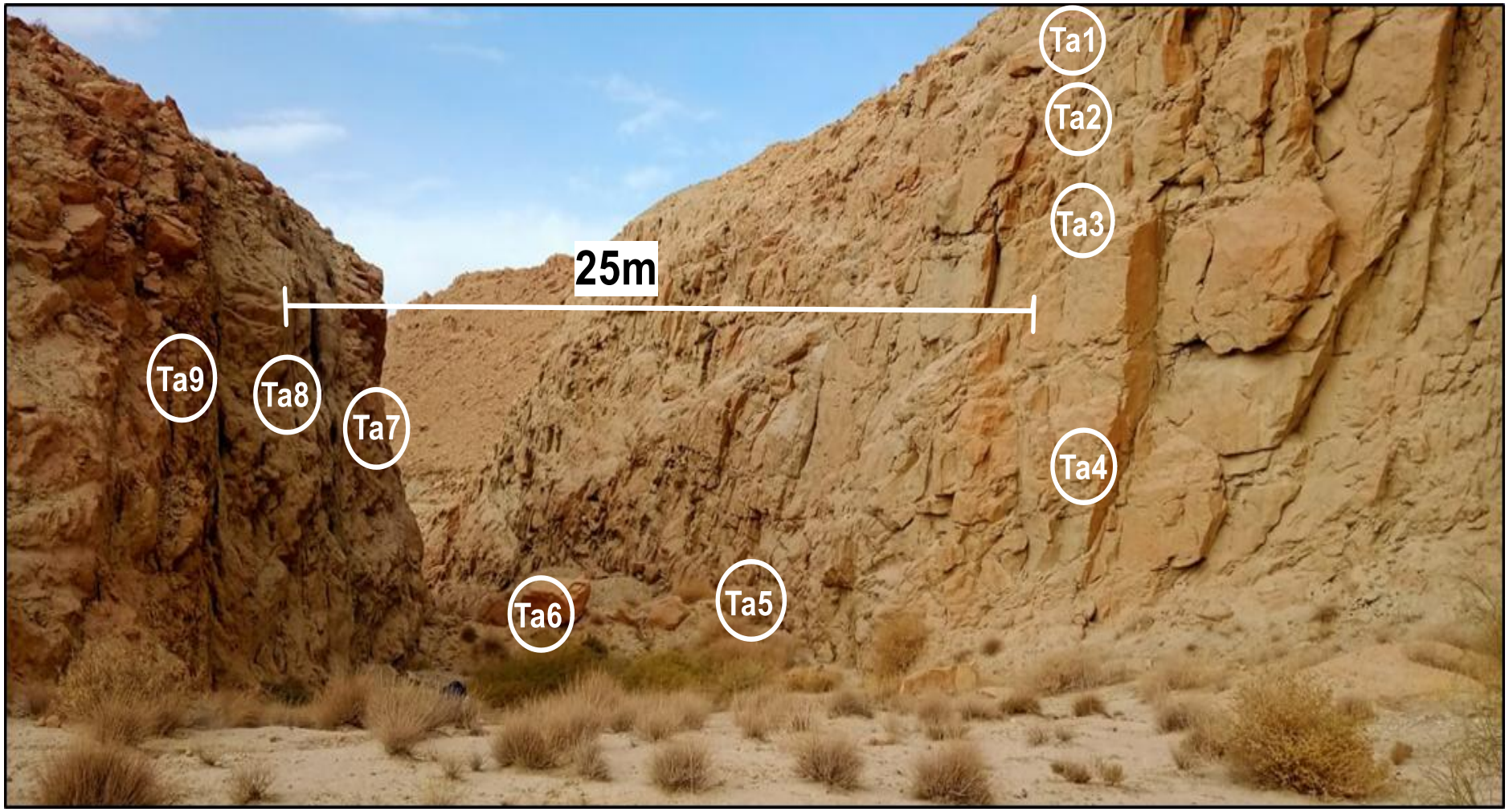

Fig. 11: Field photographs of samples of phosphorite outcrops in the Tarfaya deposit, which the layers are tectonically reversed structure.

Conclusion

The comprehensive geological analysis of the Djebel Onk region, with a focus on its regional and local geology, underscores its substantial economic and scientific value, particularly due to its rich phosphate deposits. This chapter has outlined the geographical context, stratigraphic sequences from the Upper Cretaceous to the Quaternary, and the complex structural and tectonic evolution of the area. The stratigraphy reveals a detailed sedimentary record, highlighting significant lithological variations and the presence of phosphate-rich horizons, especially within the Upper Thanetian, which is crucial for phosphate mining.

Structurally, the region is shaped by multiple phases of tectonic activity, resulting in distinct anticlines, synclines, and fault systems that influence the distribution and morphology of the phosphate deposits. The mineralogical and petrographic studies further support the economic potential of the region, identifying high-quality phosphate ores with commercial P_2O_5 content.

The local geological assessments at Kef Essenoun and Tarfaya deposits reinforce the regional geological framework, demonstrating consistent stratigraphic formations and tectonic characteristics. These insights not only enhance the understanding of the geological history and resource distribution in the Djebel Onk basin but also serve as a vital foundation for guiding sustainable exploration and exploitation strategies in northeastern Algeria.

CHAPTER III

PETROGRAPHIC, MINERALOGICAL, AND GRAIN SIZE OF PHOSPHATE

CHAPTER III

PETROGRAPHIC, MINERALOGICAL, AND GRAIN SIZE OF PHOSPHATE

Introduction

This chapter presents a comprehensive petrographic, mineralogical, and grain size investigation of phosphatic sediments collected from the Tarfaya deposit. The objective is to analyze the compositional and textural attributes of the phosphate layers (basal, main, and upper) to better understand their depositional environments and diagenetic histories. A total of nine representative samples were collected from marl, phosphate, and limestone layers and subjected to a series of laboratory techniques, including petrographic microscopy, X-ray diffraction (XRD), and grain size analysis. This multidisciplinary approach provides insights into the sedimentary structures, mineralogical composition, and particle size distribution that define the phosphate-bearing formations of the study region.

1. Sampling and methodology

1.1. Sampling

1.1.1. Sampling collection

A total of 9 samples were obtained from the Tarfaya deposit, representing the three layers: marl, phosphate, and limestone. In the phosphate layer, we have three sub-layers: the basal sub-layer, the main sub-layer, and the upper sub-layer. The following samples will be studied: (Ta1) from the marl layer, (Ta2; Ta3) for the basal layer, (Ta4; Ta5; Ta6) for the main layer, (Ta7; Ta8) for the upper layer, and (Ta9) from the limestone layer. The samples are shown in (Fig. 12).

- **Particle size classification and washing**

The sieve list used: *f* <40 µm, *f* 40 µm, *f* 63 µm, *f* 100 µm, *f* 125 µm, *f* 160 µm, *f* 250 µm, and *f* 500 µm (Fig. 13):

- Weigh 200 g of dry sample, record the weight, and transfer the sample to the 500 µm sieve and close the lid.
- Place the assembly on the mechanical agitator with a hammer and secure it.
- Shake for 15 minutes.
- Remove the assembly and unravel it.
- Weigh each sieve and the base containing a fraction of the sample.

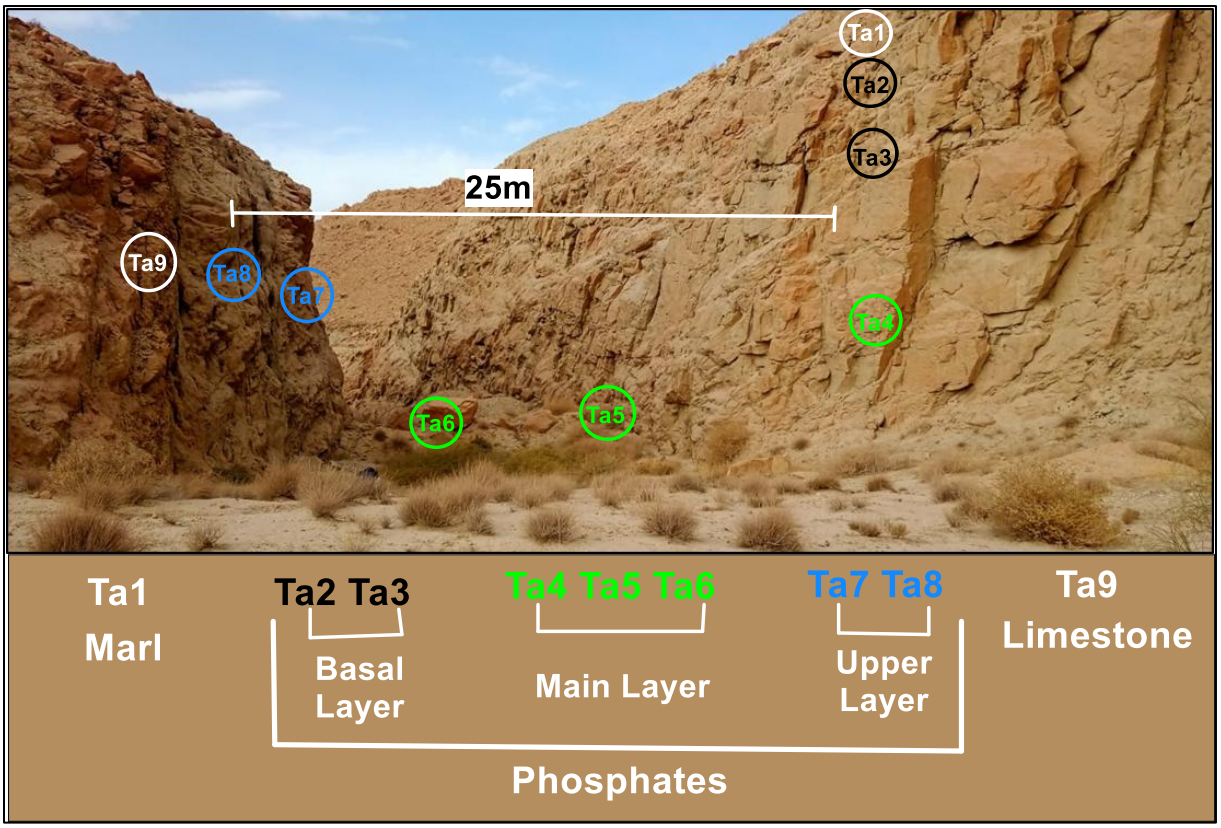

Fig.12: Subdivision of the layers and the sampling of the Tarfaya deposit, which the layers are tectonically reversed structure.

Fig.13: The series of sieves used for this study.

After sieving, the samples are left to dry at the laboratory stove before being reweighed. Finally, the samples are examined under a binocular magnifying glass to characterize the phosphate grains, glauconite, pellets, coprolites, fish teeth, and lithoclasts.

- **Laboratory processing steps**

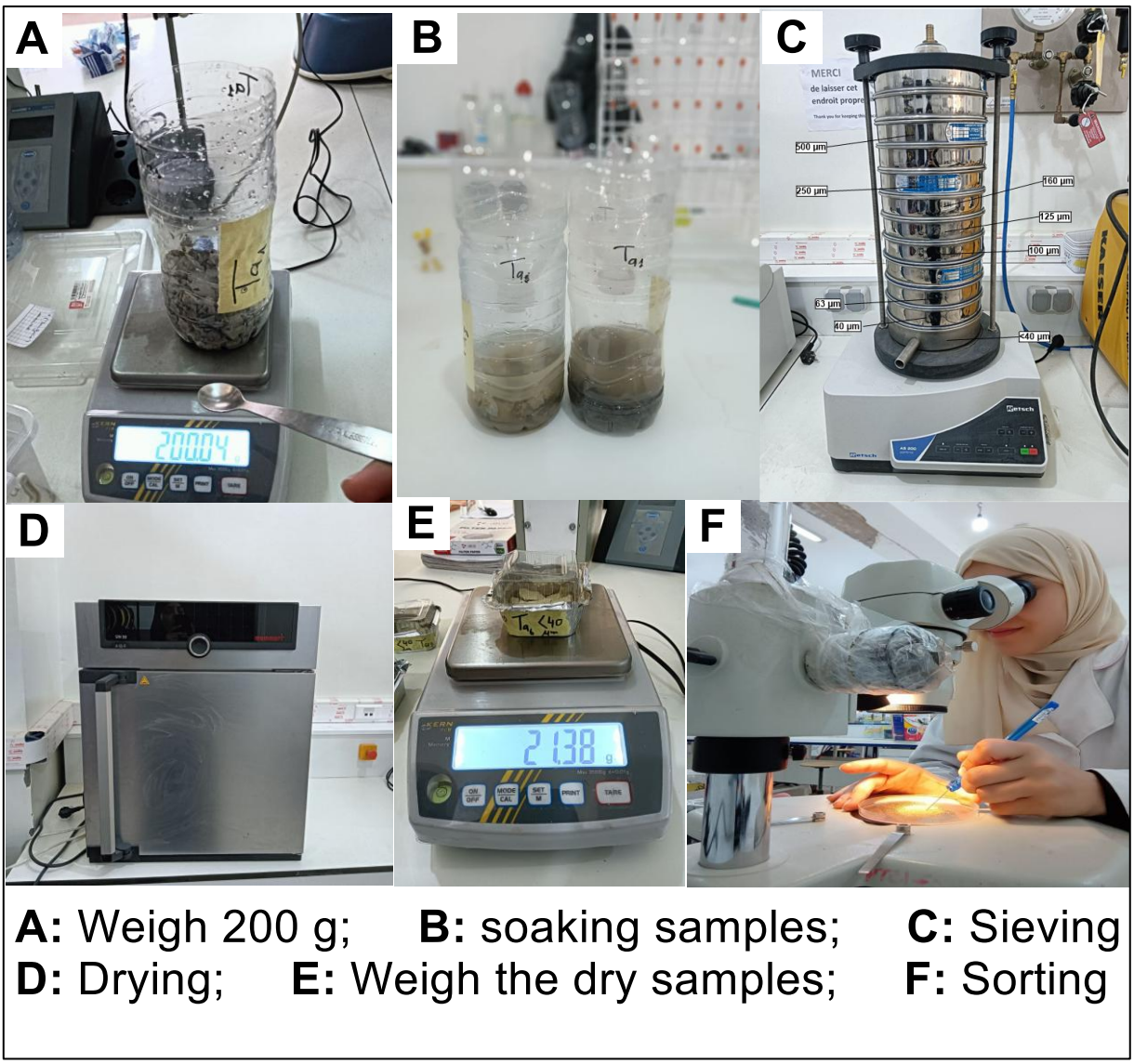

Fig.14: Laboratory processing steps.

1.2. Analytics methods

1.2.1. Petrographic analysis

Phosphate samples were collected and prepared at the Sedimentology Laboratory of the University of Ouargla. The preparation involved preliminary crushing, quartering, and soaking in distilled water to disaggregate the particles. Grain size analysis was carried out through wet sieving using a series of standardized mesh sizes, targeting specific grain-size fractions: $f < 40$

μm, *f* 40 μm, *f* 63 μm, *f* 80 μm, *f* 100 μm, *f* 125 μm, *f* 160 μm, *f* 250 μm, and *f* >500 μm. After drying and weighing the sieved fractions, the grain size data were processed using descriptive statistical methods to determine mean grain size, sorting, and skewness, aiding in the characterization of sedimentary textures. Finally, the samples were examined under a binocular microscope to identify components such as coprolites, pellets, glauconite, and bioclasts.

1.2.2. Mineralogical analysis

Sampling was carried out in the Tarfaya deposit, totaling 9 samples representative of regional lithological strata that were collected in the field. A microscopic study was carried out to describe the mineralogical character of the phosphates. To generate a better mineral diffraction diagram, the phosphate samples were ground to powder. This powder was stored in a holder on the sample XRD instrument at the Sahara Geology Laboratory (Research Center - University of Ouargla). The instrument was operated at a generator voltage of 40 kV, whose XRD characteristics are a Cu Kα radiation source with a wavelength λ of 1.540598 Å. The resulting diffractograms were used for mineralogical interpretation. The peaks obtained were carefully measured, and the minerals were recognized by converting the 2θ values into 'd' values. The characteristics of each mineral phase are recorded on a file in the form of a list of peaks. Each type of mineral has a distinct crystal structure that produces a distinct X-ray diffraction pattern, enabling rapid identification of minerals in a rock or soil sample. Applying Bragg's Law, we use the equation "$2 \times d \times \sin \theta = n \times \lambda$", which establishes a relationship between the distance between atoms in a crystal and the angles at which X-rays supplied to the crystal are predominantly diffracted. The position in 2θ is converted into an interreticular distance "d" expressed in Å. The intensity "I" of each peak is expressed in counts/s. The X-ray diffractogram obtained from an unknown sample is automatically compared with all the records in the database using software. No manual comparison was carried out to confirm the results.

The database used comprises 157,048 ASTM files. This database was published in 2004 by the International Center of Diffraction Data (ICDD) (ex-JCPDS: Joint Committee on Powder Diffraction Standards, ex-ASTM Committee E4) (Fig. 15).

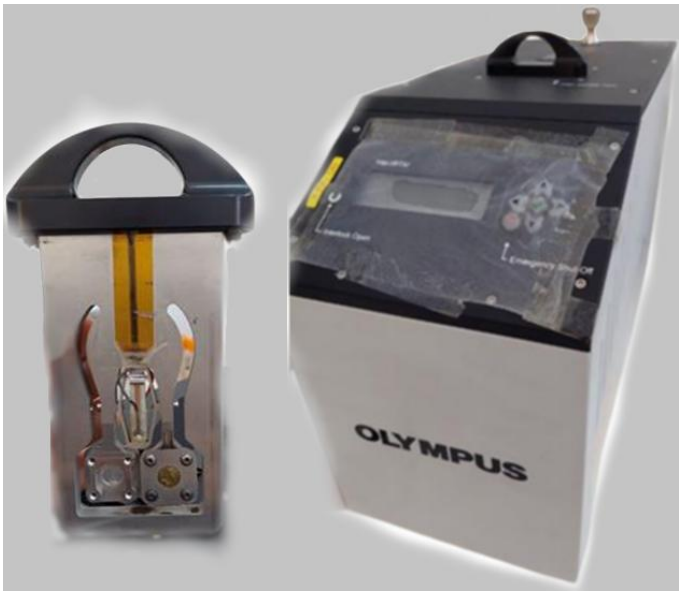

Fig.15: Photo showing the diffraction instrument used (Sahara Geology Laboratory, Ouargla University).

1.2.3. Grain size analysis

Samples were selected based on their friability and collected from different stratigraphic levels. Dry sieving was conducted to determine the relative and cumulative frequency of grain sizes. The statistical analysis involved calculating several parameters, including the mean grain size (Φ), sorting coefficient (σ), skewness index (Sk), and kurtosis index (K). Graphical tools such as grain size distribution curves and cumulative frequency curves. Based on these analyses, the samples were mainly classified as fine sand, exhibiting varying degrees of sorting and skewness. These characteristics suggest that the depositional environments were predominantly high-energy systems, such as beaches, river channels, or shallow marine shelves.

Table 1: The statistical formulas used to calculate grain size parameters.

Grain size parameters	Graphical method (Folk & Ward, 1957)	Meanings
The average	M_z= (Ø 16+ Ø 50+ Ø 84) /3 Ø16: Particle diameter, in Ø units.	
Classification (Sorting or standard deviation)	σ = ((Ø 84- Ø 16)/4) + (Ø95- Ø5)/6.6)) Ø = -log2D where D is the grain size in millimeters	0 < σ < 0.35: Very well sorted 0.35 < σ < 0.50: Well sorted 0.50 < σ < 0.71: Moderately well sorted 0.71 < σ < 1.00: moderately sorted 1.00 < σ < 2.00: Poorly sorted 2.00 < σ < 4.00: Very poorly sorted
Asymmetry (Skewness)	Ski = ((Ø16- Ø84+2.Ø50) / 2(Ø 84- Ø16)) +((Ø5+ Ø95-2. Ø50) /2.(Ø95- Ø5))	+1,00 >Ski> +0,30 : Very fine skewed +0,30 >Ski> +0,10 : Fine skewed +0,10 >Ski>-0,10 : Symmetrical -0,10 >Ski> -0,30 : Coarse skewed -0,30 >Ski> -0,10 : Very coarse skewed
Kurtosis (acuity coefficient)	K_G= (Ø95- Ø5) / (Ø75-25))	K_G< 0,67 : Very platykurtic 0,67-0,90 : Platykurtic 0,90-1,11 : Mésokurtic 1,11-1,50 : Leptokurtic 1,50-3,00 : Very leptokurtic 3,00 <K_G : Extremely leptokurtic

2. Results and discussion

2.1. Petrographical analyses

The phosphorite layer form Tarfaya deposit is stratigraphically subdivided into three (3) distinct sub-layers: basal, main, and upper.

- The basal sub-layer (Ta2 and Ta3) is characterized by a composition of approximately 50% coprolites and pellets, 1 % glauconite, 48 % carbonate cement, and a minor presence (1%) of fish teeth. (Fig. 16.A)
- The main sub-layer (Ta4, Ta5, and Ta6) exhibits a similar content of coprolites and pellets (50%), with slightly higher glauconite content (2%), reduced cement (44%), and 1% fish teeth… (Fig. 16.B)
- The upper sub-layer (Samples 7) maintains the 50% coprolites and pellets but shows an increase in glauconite (5%) and a slight decrease in cement (43%), while fish teeth remain constant at 1% (Fig. 16.C).

This vertical variation highlights subtle changes in depositional conditions and early diagenetic processes across the phosphorite sequence.

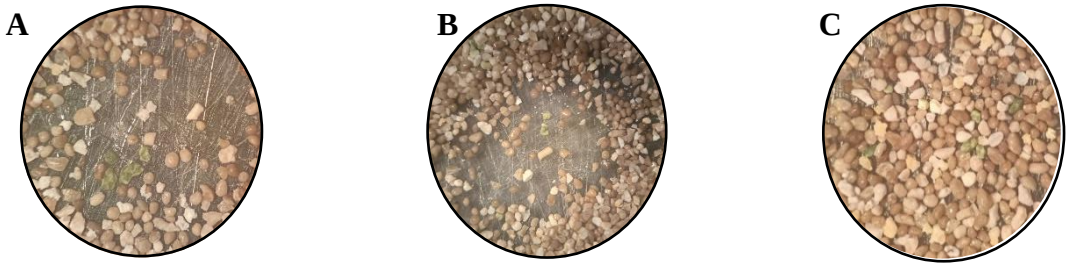

Fig.16: View under the microscope, **A:** sample 3 from the basal sub-layer, **B:** sample 5 from the main sub-layer, **C:** sample 7 from the upper sub-layer.

2.1.1. Main petrographic constituents of phosphate sediments

The petrographic composites of phosphate consist of phosphochem and matrix (and cement) as well as phosphoclastic materials, including lithoclasts and bioclasts that have been identified. Petrographic examination of the grain size fractions shows that phosphate particles are composed of the following composites:

- **Coprolites**

are fecal particles resulting from the excrement of fossil animals (Lamboy et al., 1994). Under the microscope, coprolites have different brownish colors, ranging from white to brown and almost black, and cylindrical to compressed elliptical forms. They have variable diameters, generally exceeding 250 μm and reaching up to a few millimeters (Fig. 17). Coprolites contain various preserved organic and mineral inclusions. Siliceous and dolomitic inclusions have been identified in coprolites from the Tébessa region and have been interpreted as the result of diagenetic processes, such as burial and sedimentary reworking, which in some cases were

responsible for micro-fracturing of the particles (Kechiched et al., 2020). Coprolites can coexist with pellets, showing poor classification. Kechiched, 2017.

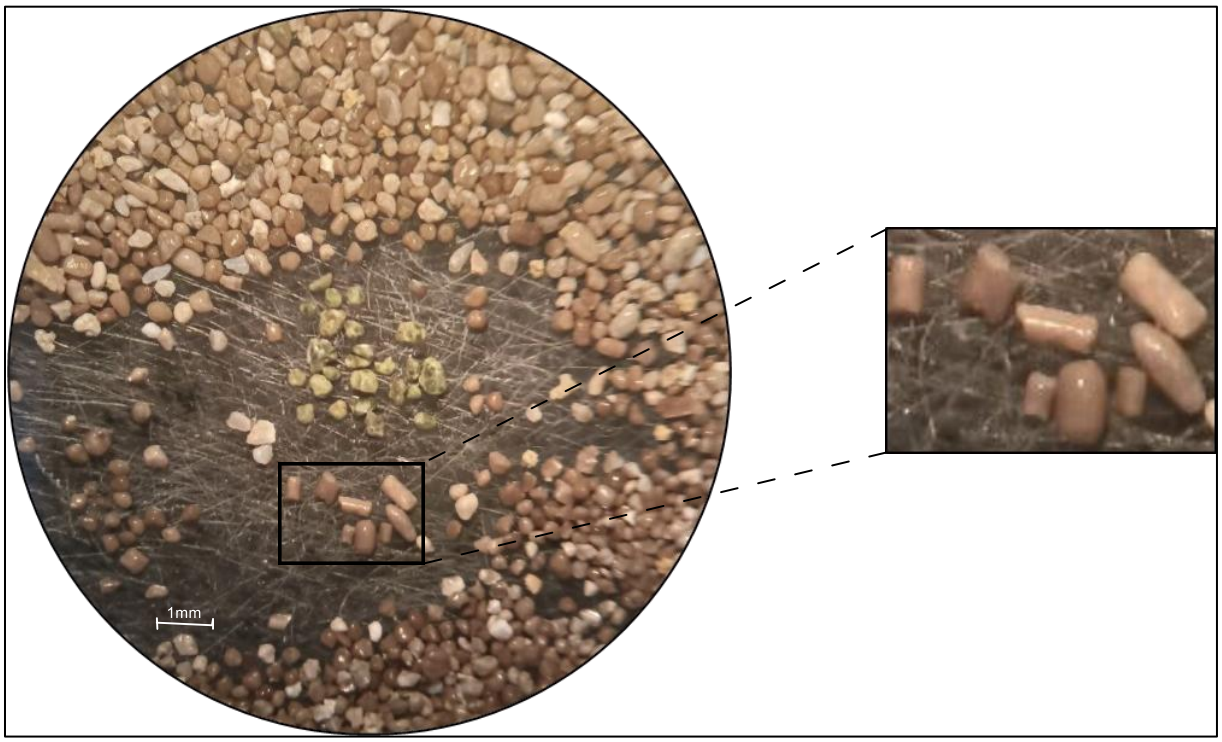

Fig.17: Petrographic constituents of phosphate under the microscope. Phosphate grains (pellets, coprolites) separated from the cement, showing a "blunt, shiny" smooth morphology in the presence of glauconite.

- **Pellets**

Phosphate pellets are products of fecal origin. Pellets are permanent and dominate phosphate mineral particles in the Tébessa region, with a higher concentration in the south than in the north (Kechiched, 2017). Under the microscope, pellets are ovoid or rounded in form and show a smooth surface due to the effect of reworking, with diameters generally varying from 200 µm to 250 µm (Fig. 18). The fragmentation of pre-existing coprolites by sedimentary reworking leads to the formation of particles with high porosity compared to coprolites, which are pellets (Chabou-Mostefai, 1987; Ben Hassen et al., 2010; Kechiched et al., 2020). In addition, the reworking and remobilization of coprolites led to the gluconitization process of the particles (Kechiched et al., 2018).

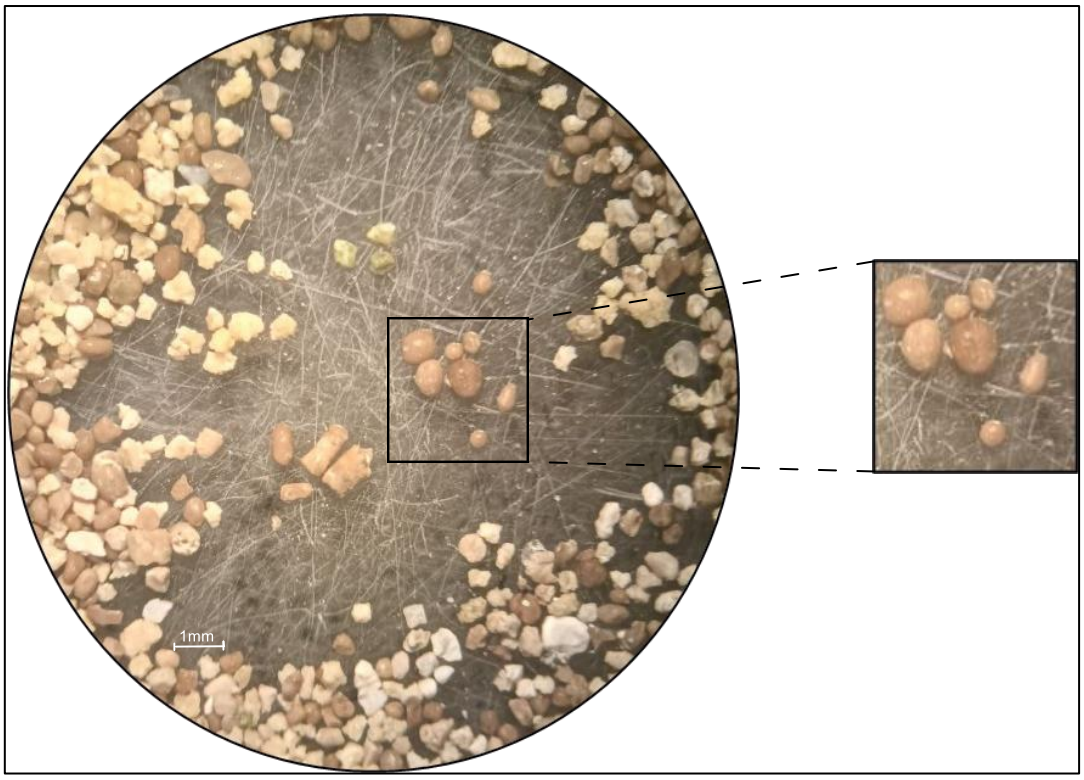

Fig.18: Petrographic constituents of phosphate. Phosphate grains (pellets, coprolites) separated from the cement, showing a smooth morphology in the presence of glauconite.

- **Glauconite**

Glauconite has a greenish color and varies in size from a few hundred micrometers to over 1 mm (Fig. 19). It is often distributed between grains (intergranular).

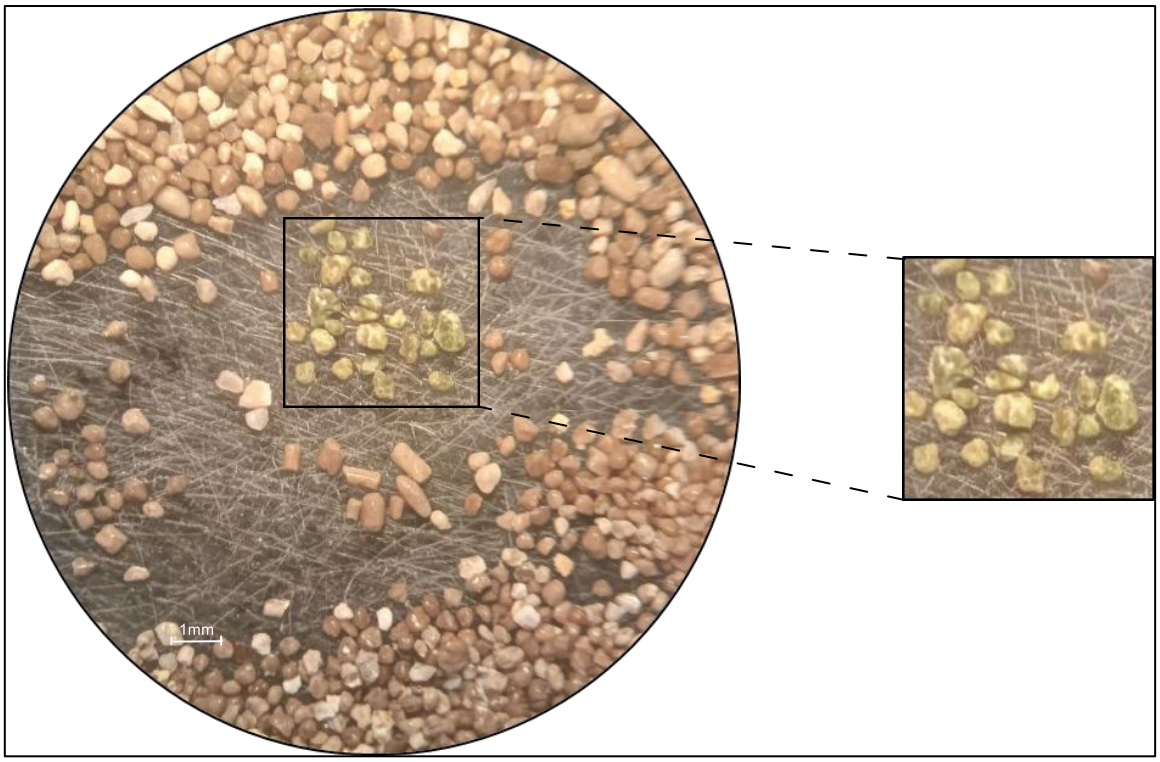

Fig.19: Petrographic constituents of phosphate under the microscope. Phosphate grains (glauconites, pellets, and coprolites) separated from the cement, showing the morphology of glauconite.

2.2. Mineralogical analyses

X-ray diffraction (XRD) analysis revealed that the studied sample is primarily composed of carbonate fluorapatite (CFA), as indicated by strong diffraction peaks at d-spacings of 3.488 Å, 2.935 Å, 2.709 Å, and 2.232 Å. This mineral represents the main phosphate phase within the samples, which is consistent with characteristics typically observed in sedimentary phosphate deposits.

In addition to CFA, several accessory minerals were identified, such as quartz (Qz), with peaks at 3.648 Å, 2.441 Å, and 1.815 Å, and dolomite (Dol), with peaks at 2.826 Å, 2.034 Å, and 1.950 Å. The presence of hulsite (?) is suggested by peaks at 5.084 Å and 4.732 Å, though these assignments are tentative.

These results confirm that carbonate fluorapatite is the dominant phase, while the matrix is largely composed of dolomite and quartz. Such mineralogical associations are commonly reported in Algerian-Tunisian phosphate formations (Chabou-Mostefai, 1987; Cielensky et al., 1988; Bezzi et al., 2012; Galfati et al., 2010).

The analysis was carried out on the fine fraction (<45 µm), which enhances the detection of major and accessory crystalline phases. The distinct presence of dolomite at d = 2.826 Å and quartz at d = 3.648 Å and 2.441 Å is notable in this fine fraction. The absence of some secondary peaks may be attributed to low crystallinity or trace concentrations of those phases.

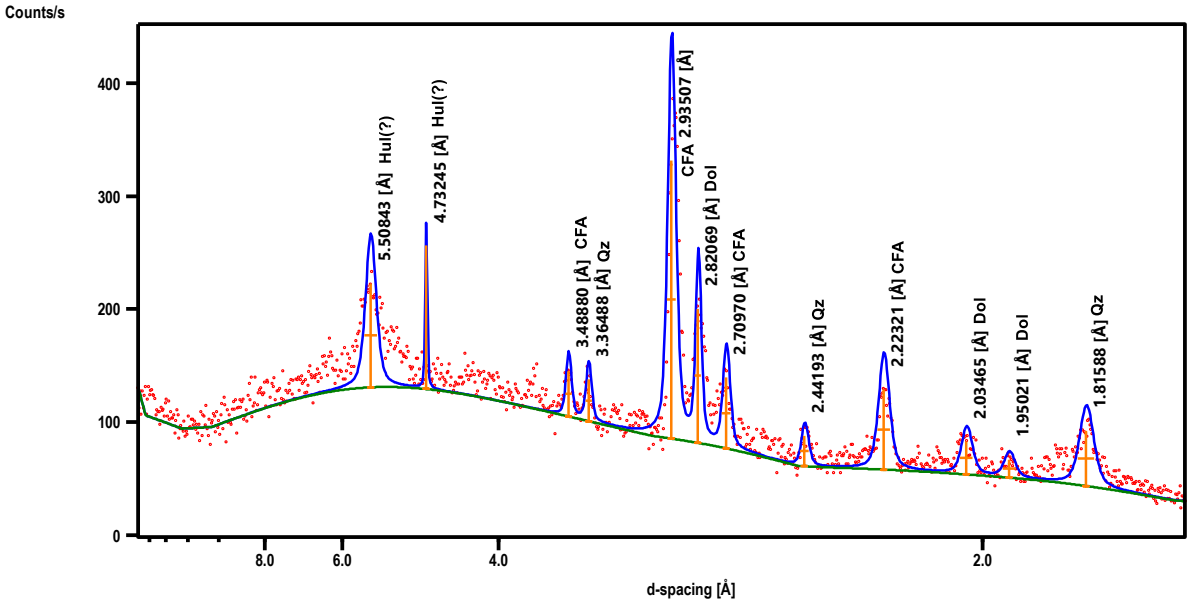

Fig.20: XRPD patterns of phosphorite samples showing the main phosphorite.

CFA = carbonate fluor-apatite, **Dol** = dolomite, **Qz** = quartz, **Hul** = heulandite, **d** = d spacing values (Å). The most intense reflection of each mineral is in bold.

2.3. Grain size analyses

The aim of this chapter is to study the grain size characteristics of sedimentary phosphates from the Tarfaya deposit (Djebel Onk).

2.3.1. Phosphate minerals from the Tarfaya deposit (Tébessa South)

Six (6) phosphate samples (from the base to the upper of the deposit) were taken for the grain size analysis of phosphate ore from the Tarfaya deposit. The samples represent the phosphate levels of the basal layer (Ta2-Ta3), the main layer (Ta4-Ta5-Ta6), and the upper layer (Ta7). These samples were selected on the basis of their friability, making them suitable for the different grain size treatments. Folk and Ward (1957) indices were calculated using a programmed GRADISTAT spreadsheet (Simon, 2010).

2.3.2. Basal layer

The sieving results for samples Ta2 and Ta3 are mentioned represents:

Table 2: Table of relative frequencies and cumulative frequencies for samples Ta2 and Ta3 (unit %)

	Diameters (µm)	<40µm	40 µm	63 µm	100 µm	125 µm	160 µm	250 µm	500 µm
Ta2	Relative frequencies	9.57	2.567	3.99	1.26	5.54	18.50	12.16	46.40
	Cumulative frequencies	9.57	12.13	16.13	17.39	22.93	41.44	53.60	100.00
Ta3	Relative frequencies	20.39	7.66	16.45	6.93	35.48	10.82	1.40	0.87
	Cumulative frequencies	20.39	28.05	44.50	51.43	86.91	97.73	99.13	100.00

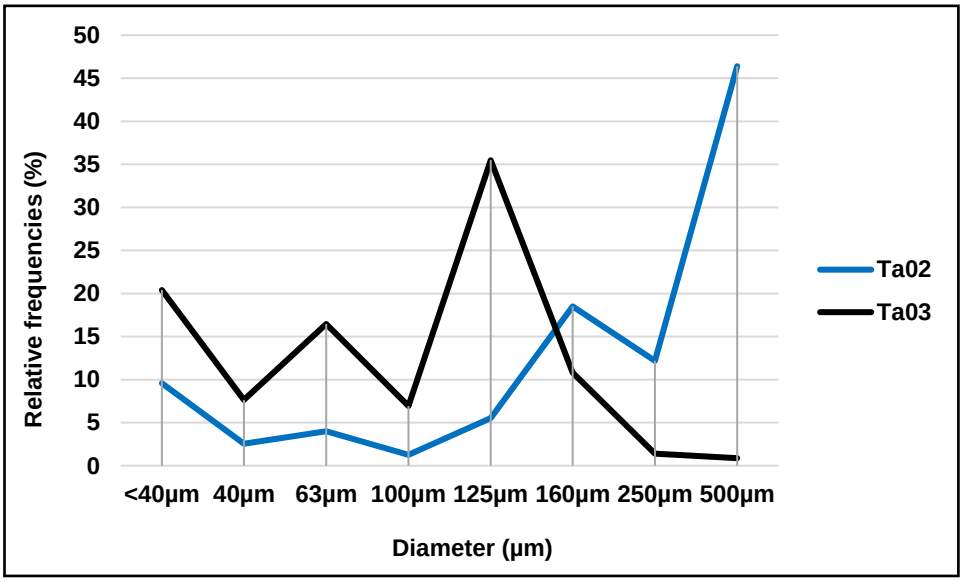

Fig.21: Relative frequency curves for the basal layer.

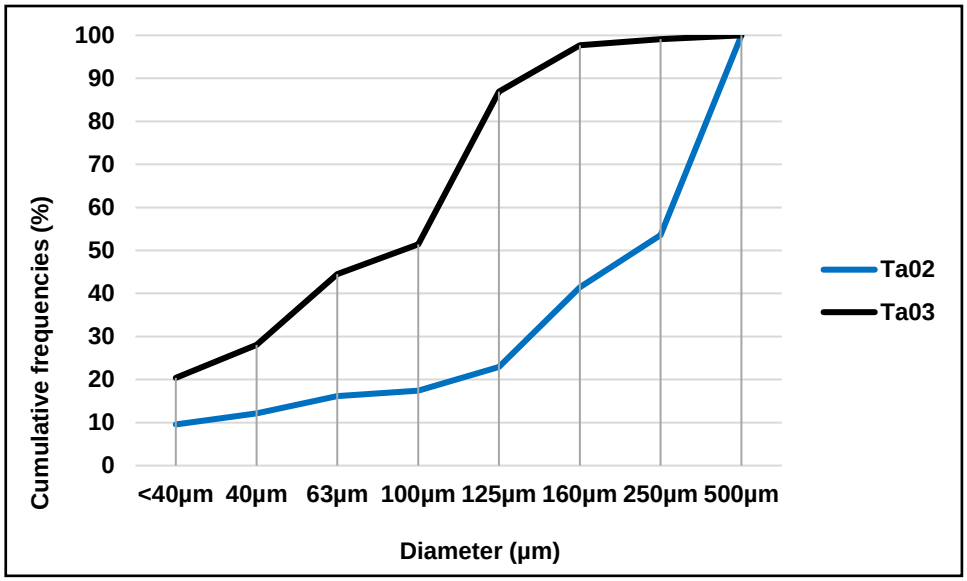

Fig.22: Cumulative frequency curves for basal layer samples.

The relative frequency curves (Fig. 21) show a monomodal distribution for both samples. Ta2 shows an abundance of the *f* 500 µm fraction with about 45 %. In contrast, Ta3 peaks at the *f* 125 µm fraction, showing a broader and finer distribution, about 35 %.

The cumulative frequency curves (Fig. 22) indicate that Ta3 reaches nearly 100 % at *f* 250 µm. On the other hand, Ta2 only reaches 100% at *f* 500 µm. At the *f* 125 µm fraction, Ta3 shows a cumulative percentage of approximately 80 %, while Ta2 ranges only between 20 and 25 %.

- **Grain size parameters**

(1) The mean grain size is 185.8 µm, which corresponds to values between approximately 2.4 and 2.5 on the *phi* (φ) scale. This indicates the sediment is composed of fine sand, likely resulting from moderate-energy depositional environments.

(2) The sorting coefficient (σ) is 2.230, indicating that the sample is poorly sorted. This means that the grain sizes are diverse and not uniform, which could reflect variable transport or depositional conditions.

(3) The skewness index (Sk) is -0.010, showing a symmetrical distribution, meaning there is no dominant trend toward either finer or coarser grains.

(4) The kurtosis index (K) is 1.026, which is considered mesokurtic. This suggests a normal distribution of grain sizes with moderate peakedness, reflecting a balanced range of sizes without excess of extremes.

- **Grain Size Analysis**

- **Grain Size Characteristics and Statistical Parameters (Figs. 23–25)**

Based on the statistical data (Fig. 23), the mean grain size is approximately 2.61 Φ, equivalent to about 153 microns, categorizing the sediment as fine sand. The sorting value of 0.66 Φ indicates moderately well-sorted sediment, suggesting a relatively uniform grain size distribution with minor variations. The skewness of -0.12 implies a slight dominance of coarser particles, making the distribution slightly coarse-skewed. Kurtosis is calculated at 0.89, identifying the curve as platykurtic, or flat, which denotes a broad range of particle sizes. The grain size distribution (Fig. 24) exhibits a major peak between 150 and 200 microns, reinforcing the classification as fine sand. Additionally, there is a minor presence of particles finer than 100 microns, indicative of silt, while coarse and gravel-sized particles are absent. The cumulative curve (Fig. 25) shows D10 at approximately 90 microns, D50 (median) around 153 microns, and D90 at about 260 microns, yielding a sorting range (D90 - D10) of roughly 170 microns. This range supports the conclusion that the sediment includes fine to medium sand with a consistent texture and moderate sorting.

- **Final Interpretation and Environmental Implications**

The sediment sample is best classified as fine sand that is moderately well sorted and slightly coarse-skewed, with minimal fines and no gravel-sized material. These textural properties, when considered in the context of phosphate sedimentation, suggest deposition in a high-energy marine environment where dynamic hydrodynamic conditions prevail. Such settings facilitate the concentration of phosphate grains by winnowing away finer particles and preventing the accumulation of coarser clasts. The observed grain size distribution supports a reworked phosphate deposit, where wave or current action selectively concentrates phosphatic particles of similar size, leading to the moderately well-sorted texture. The slight coarse skewness may reflect episodic input of slightly larger phosphate fragments or shell debris. Overall, the sedimentary characteristics are consistent with a high-energy, shallow marine depositional system conducive to the formation and concentration of economic phosphate deposits.

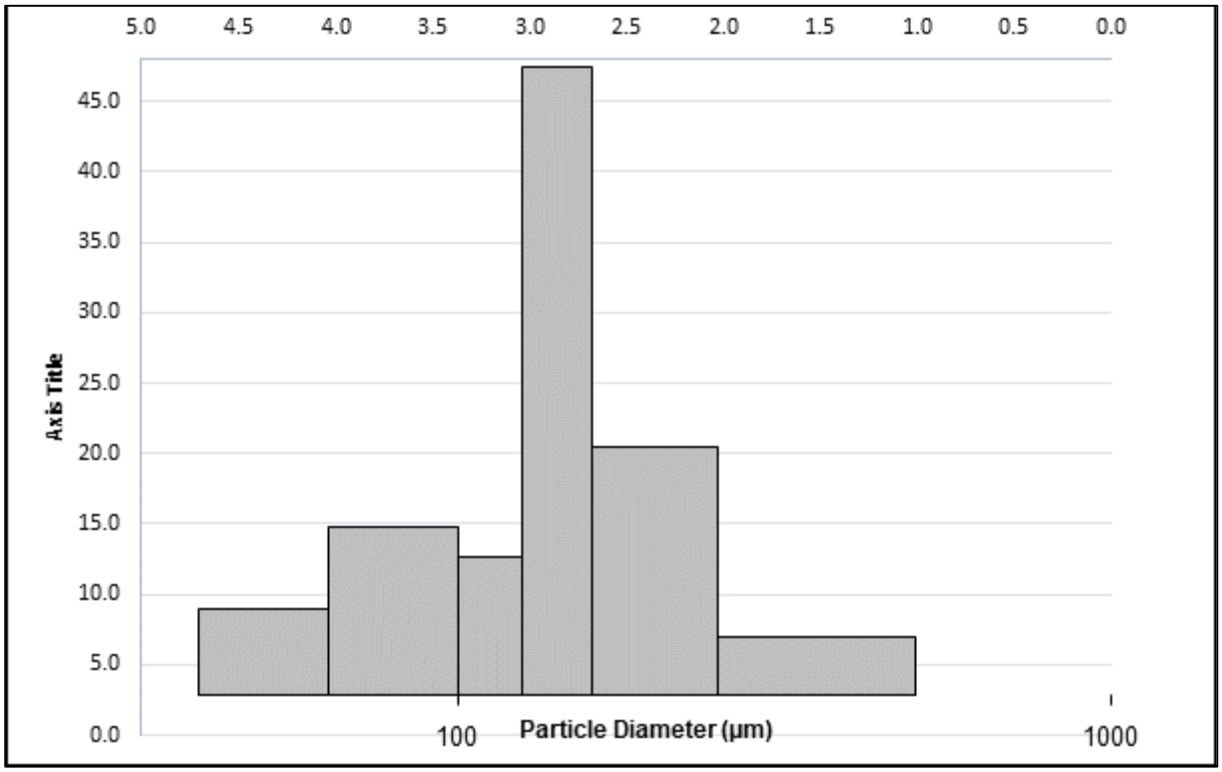

Fig.23 : Grain size distribution of Basal Layer.

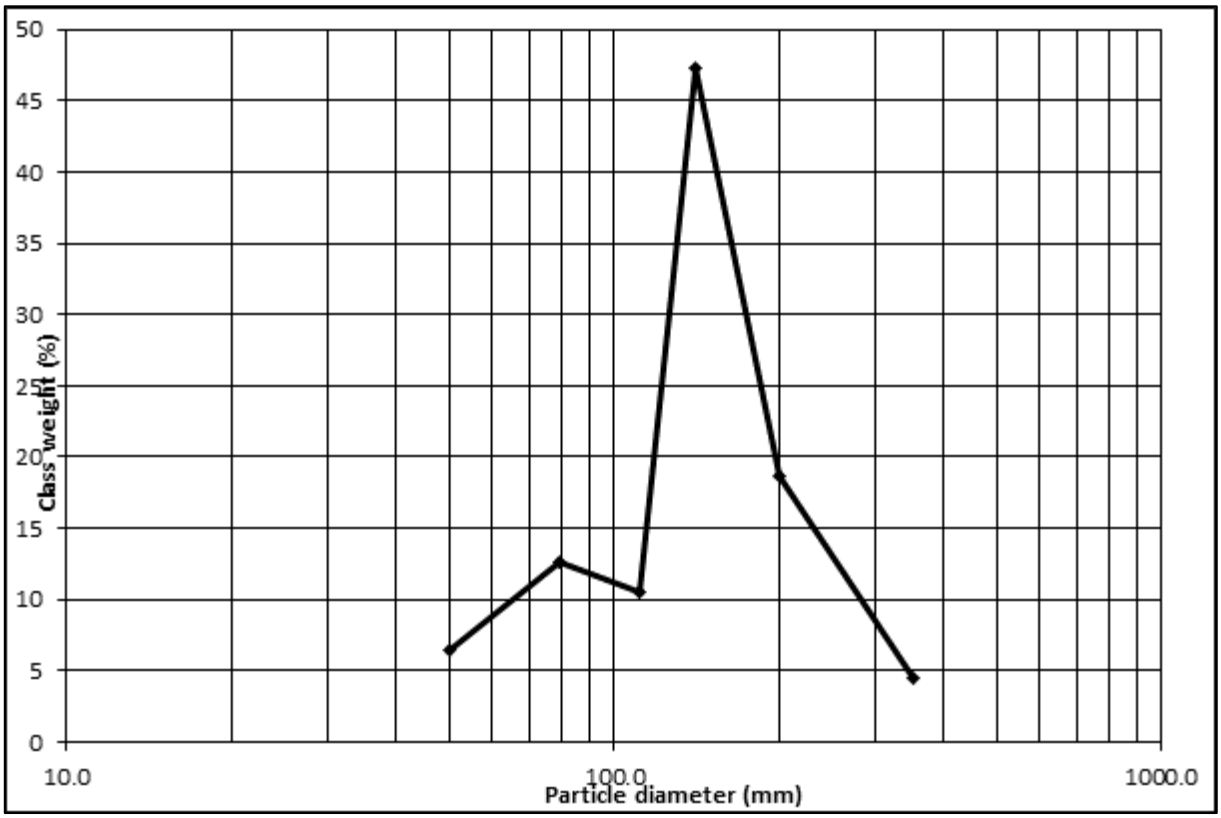

Fig.24: Distribution (microns) of Basal Layer.

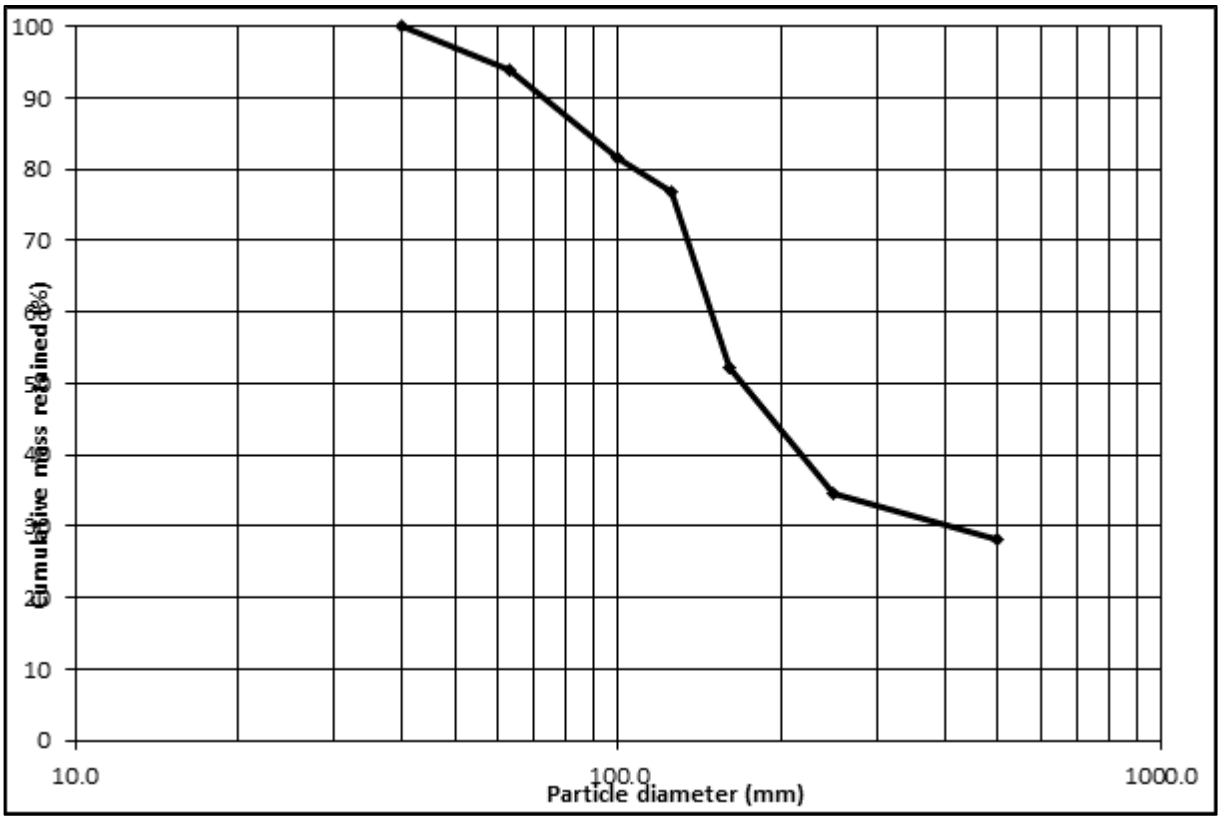

Fig.25: Cumulative (microns) of Basal Layer.

2.3.3. Main layer

Grain size analysis was carried out on samples Ta4, Ta5 and Ta6. These samples show an abundance of phosphate grains in general (Table 3).

Table 3: Table of relative frequencies and cumulative frequencies for samples Ta4, Ta5 and Ta6 (Unit %).

	Diameters (µm)	**<40µm**	**40µm**	**63µm**	**100µm**	**125µm**	**160µm**	**250µm**	**500µm**
Ta4	Relative frequencies	17.40	6.26	9.58	3.69	17.76	27.75	16.76	0.80
	Cumulative frequencies	17.40	23.66	33.24	36.94	54.70	82.45	99.20	100.00
Ta5	Relative frequencies	8.18	2.42	2.80	1.99	4.11	16.88	60.54	3.07
	Cumulative frequencies	8.18	10.60	13.40	15.39	19.50	36.38	96.93	100.00
Ta6	Relative frequencies	19.69	6.97	12.30	3.77	12.40	29.39	14.24	1.23
	Cumulative frequencies	19.69	26.66	38.96	42.73	55.13	84.52	98.77	100.00

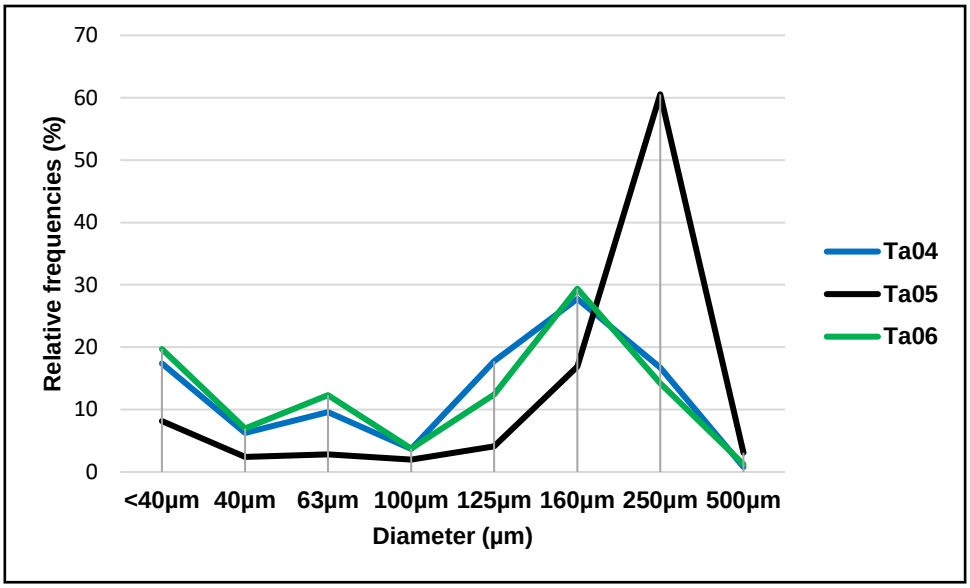

Fig.26: Relative frequency curves for main layer samples.

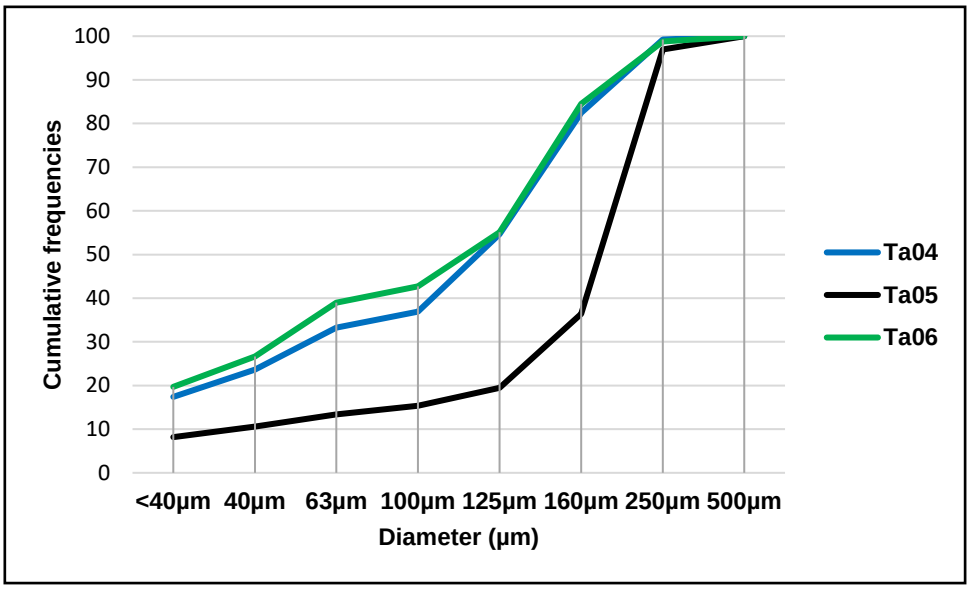

Fig.27: Cumulative frequency curves for main layer samples.

The relative frequency curves (Fig. 26) show a monomodal distribution for all three samples (Ta4, Ta5, and Ta6). Sample Ta5 shows a clear peak at the 250 µm fraction with about 60%. In contrast, Ta4 and Ta6 show broader distributions, with peak values between 160 µm and 250 µm.

The cumulative frequency curves (Fig. 27) indicate that all three samples reach nearly 100% at the 500 µm fraction. Ta4 and Ta06 display a more gradual cumulative increase, achieving around 80–85% at the 250 µm fraction. Conversely, Ta5 accumulates rapidly between 160 µm and 250 µm, reaching nearly 100% within that narrow range.

- **Grain size parameters**

(1) The mean grain size is 235.0 μm, which corresponds to approximately 2.09 φ on the phi scale. This indicates that the sediment belongs to the fine sand class.

(2) The sorting coefficient (σ) is equal to 1.885, indicating a moderate sorting of particles, reflecting some variability in grain size.

(3) The skewness index (Sk) is equal to -0.377, indicating a very fine skewed distribution, meaning a slight dominance of coarser particles in the sample.

(4) The kurtosis index (K) is equal to 0.888, which reflects a platykurtic distribution, suggesting a relatively flat grain size curve with less peakedness.

- **Grain Size Analysis**

- **Grain Size Characteristics and Statistical Parameters (Figs. 28–30)**

According to the statistical parameters (Fig. 28), the mean grain size of the sample ranges from approximately 2.4 to 2.5 Φ, equivalent to about 170–180 microns, placing it within the fine sand category. The sorting, measured between 0.6 and 0.7 Φ, indicates that the sediment is moderately well sorted, implying a relatively uniform grain size with limited variability. The skewness value is close to 0, suggesting a nearly symmetrical grain size distribution, while the kurtosis of approximately 1.0 categorizes the distribution as mesokurtic—indicating a normal, bell-shaped curve with moderate peakedness. The grain size distribution curve (Fig. 29) is unimodal, with the dominant particle sizes falling between 150 and 200 microns. There is minimal presence of both finer silt or clay particles and coarser gravel particles, confirming the uniform texture dominated by fine sand. From the cumulative curve (Fig. 30), the D10, D50, and D90 values are approximately 90–100, 170–180, and 270–300 microns, respectively. This results in a sorting range (D90 - D10) of about 170–210 microns, supporting the interpretation of moderate sorting with grain sizes spanning from fine to medium sand and a generally consistent texture.

- **Final Interpretation and Environmental Implications**

The sediment sample is primarily composed of fine sand, exhibiting moderate sorting, a unimodal and nearly symmetrical grain size distribution, and minimal silt or clay content. These sedimentary characteristics suggest deposition in a high-energy, shallow marine environment favorable for the formation and concentration of phosphate sediments. The uniform grain size and absence of gravel indicate reworking by consistent hydrodynamic processes, such as wave or current action, which efficiently remove both finer and coarser fractions. This winnowing process tends to concentrate phosphate particles within the fine- to medium-sand size range, leading to the observed moderately well-sorted texture. The mesokurtic distribution further supports stable energy conditions and minimal post-depositional disturbance. Overall, the data indicate a dynamic yet stable depositional environment typical of phosphogenic settings where biological productivity, sediment reworking, and chemical conditions align to favor the accumulation of phosphate-rich sediments.

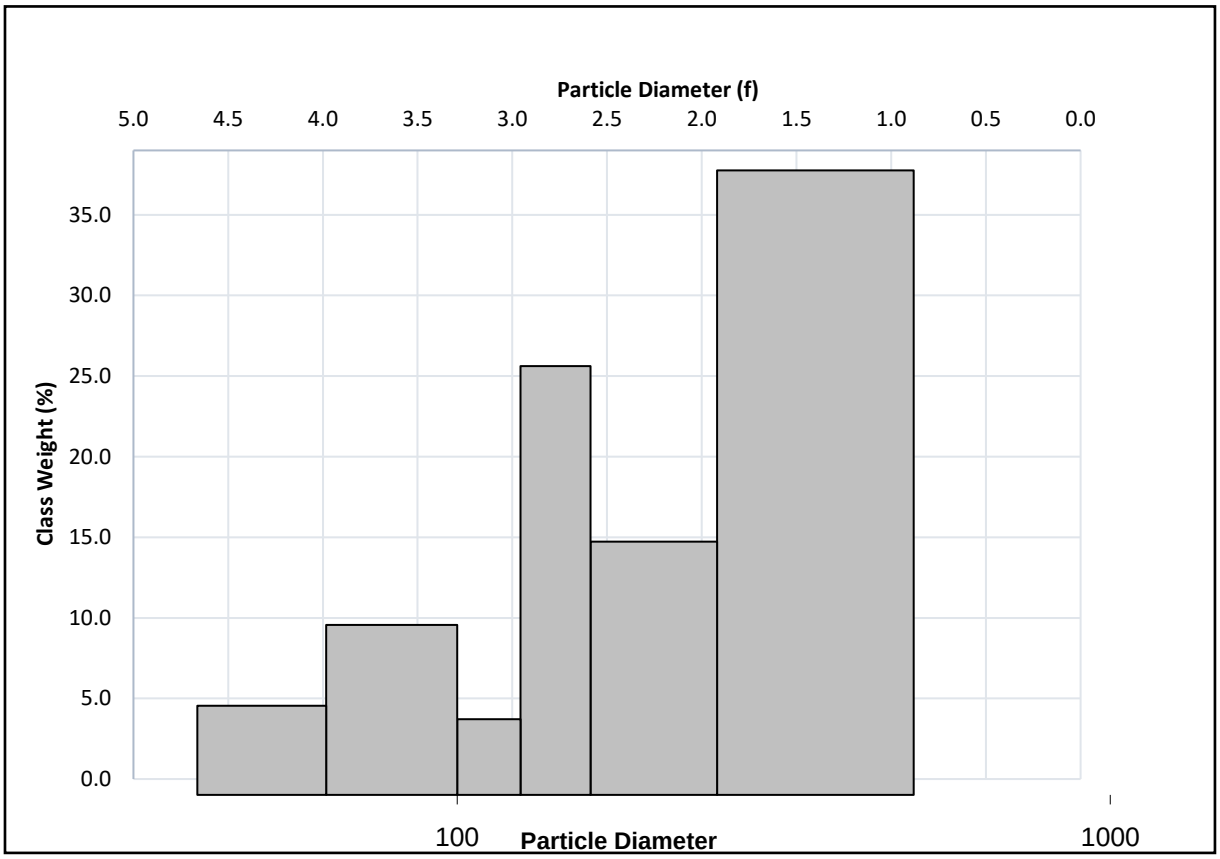

Fig.28: Grain size distribution of Main Layer.

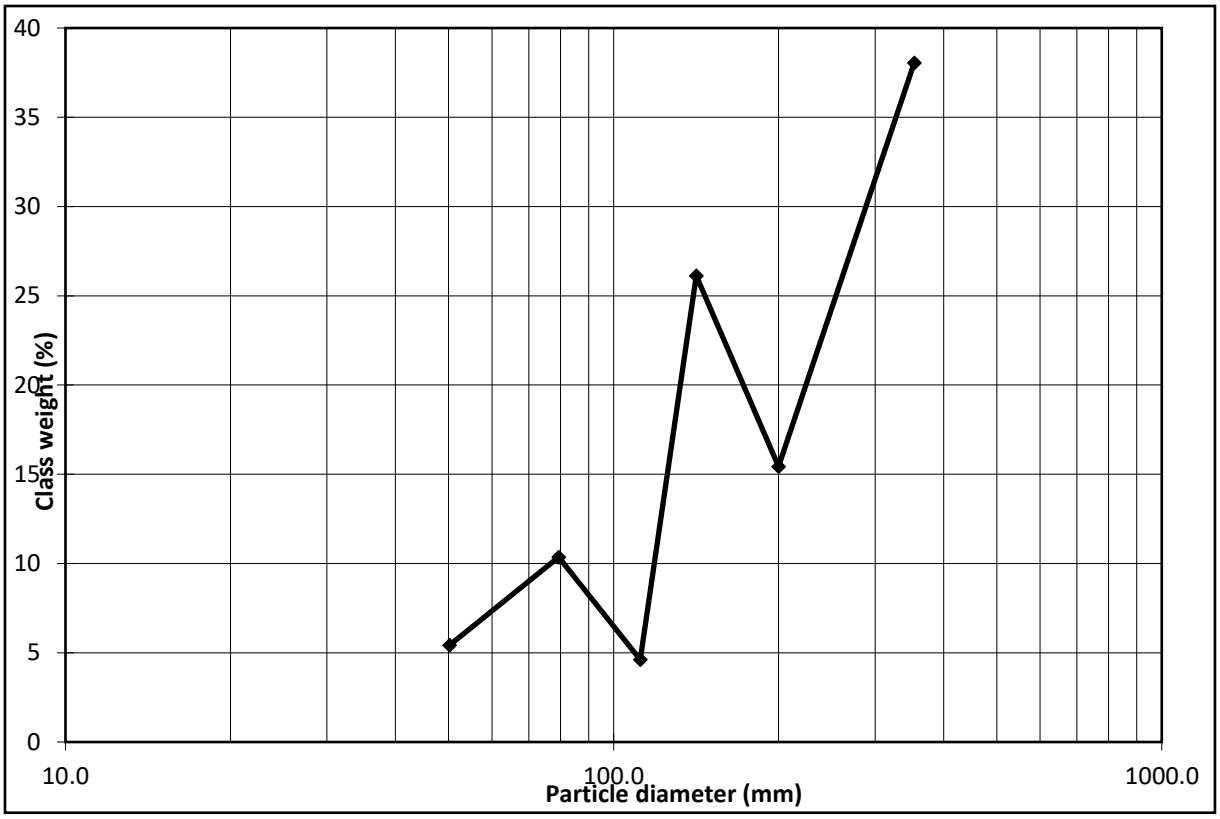

Fig.29: Distribution (microns) of Main Layer.

Fig.30: Cumulative (microns) of Main Layer.

2.3.4. Upper layer

The grain size analysis of a sample (Ta7) taken from the upper layer is presented in Table 4 and the figures (Fig. 35, Fig. 36).

Table 4: Table of relative frequency and cumulative frequencies for the sample Ta07 (Unit %).

	Diameters (µm)	<40µm	40µm	63µm	100µm	125µm	160µm	250µm	500µm
Ta7	Relative frequencies	22.19	6.75	10.32	3.46	11.64	18.37	19.92	7.34
	Cumulative frequencies	22.19	28.93	39.26	42.72	54.36	72.73	92.66	100.00

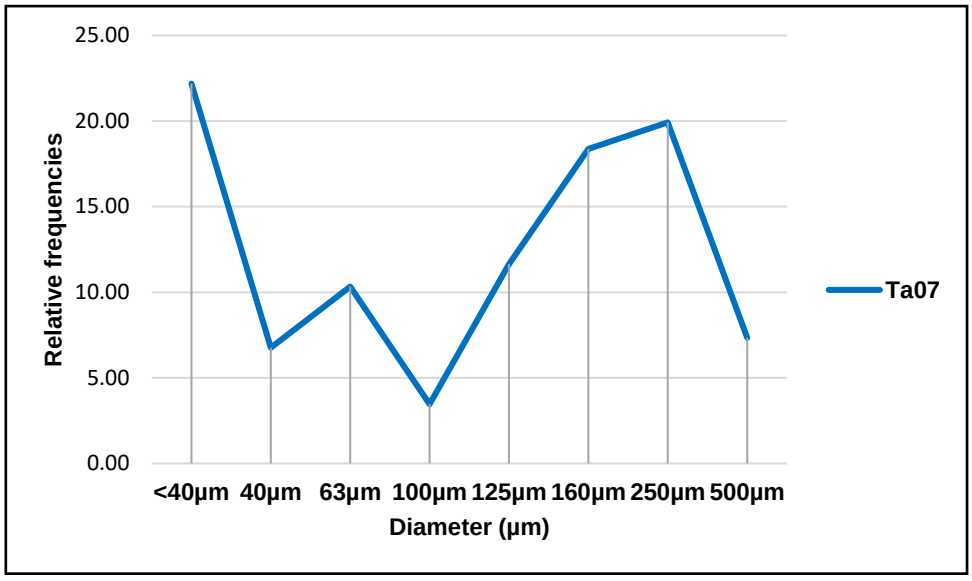

Fig.31: Relative frequency curves for upper layer samples.

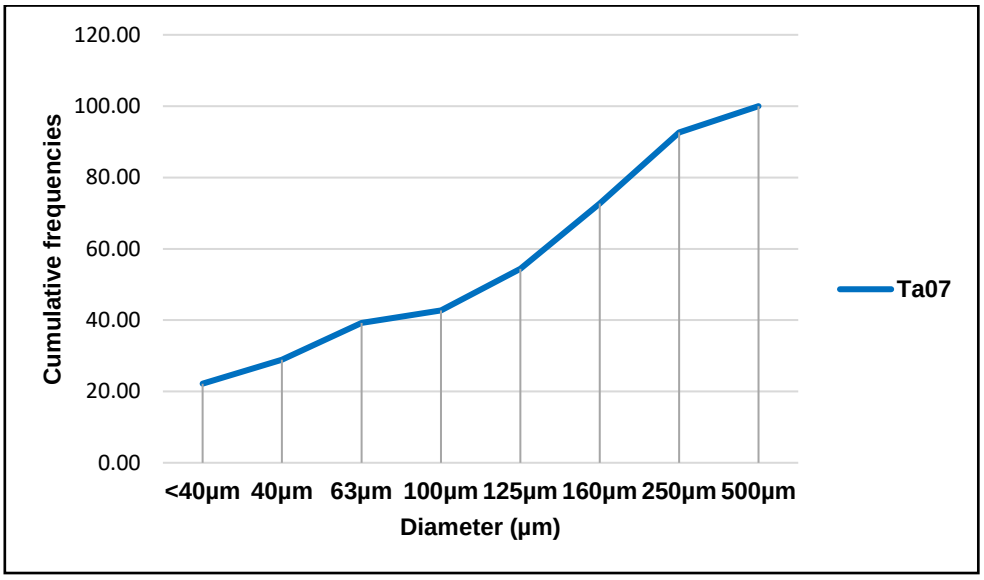

Fig.32: Cumulative frequency curves for upper layer samples.

The relative frequency curve (Fig. 31) for sample Ta7 shows a multimodal distribution, with many noticeable peaks. The highest peak is observed at the <40 µm fraction, reaching nearly 22%, followed by another significant peak at 250 µm with 20%. Others show moderate increases around 63 µm and 160 µm.

The cumulative frequency curve (Fig. 32) indicates that the sample reaches nearly 100% at 500 µm. At 125 µm, the cumulative percentage is around 50%

- **Grain size parameters**

(1) The mean grain size is 185.8 µm, which corresponds approximately to 2.42 φ on the phi scale. This places the sediment in the fine sand category.

(2) The sorting coefficient (σ) is 2.230, indicating that the sample is poorly sorted, which means it contains a wide range of grain sizes.

(3) The skewness index (Sk) is -0.010, indicating a symmetrical grain size distribution, with no strong dominance of finer or coarser particles.

(4) The kurtosis index (K) is 1.026, which indicates a mesokurtic distribution, reflecting a normal peakedness in the grain size distribution.

- **Grain Size Analysis**

- **Grain Size Characteristics and Statistical Parameters (Figs. 33–35)**

The grain size analysis (Fig. 33) reveals that the mean grain size ranges from approximately 2.3 to 2.4 Φ, corresponding to about 180–190 microns, which classifies the sediment as fine sand. The sorting, measured at around 0.6 Φ, indicates that the sediment is moderately well sorted, reflecting a relatively uniform grain size distribution. The skewness is approximately zero, suggesting a nearly symmetrical grain size distribution without a strong bias toward finer or coarser particles. Kurtosis is near 1.0, which characterizes the distribution as platykurtic, indicating a flatter-than-normal distribution curve. The grain size distribution (Fig. 34) shows a dominant peak between 150 and 200 microns, with a minor presence of finer particles below 100 microns, representing silt. Coarse or gravel-sized grains are not significantly present, which reinforces the interpretation of a sediment dominated by fine sand with minimal variation. The cumulative curve (Fig. 35) displays D10, D50, and D90 values of approximately 100, 180, and 270 microns, respectively. The resulting sorting range (D90 - D10) of about 170 microns supports the conclusion that the sediment contains grain sizes spanning from fine to medium sand with a generally consistent texture and moderate sorting.

- **Final Interpretation and Environmental Implications**

The analyzed sediment is primarily composed of fine sand with moderate sorting, a nearly symmetrical grain size distribution, and a platykurtic profile. These characteristics suggest deposition in a high-energy, shallow marine environment conducive to the formation and concentration of phosphate sediments. The absence of gravel and the low content of fines indicate effective hydrodynamic sorting, typical of settings where wave and current action winnow out finer particles and prevent the accumulation of coarser clasts. Such conditions are ideal for the concentration of phosphatic grains, which often fall within the fine to medium sand size range. The unimodal distribution peak between 150 and 200 microns reflects a stable sediment supply and consistent depositional energy, both of which are commonly associated with inner shelf or platform settings during periods of phosphogenesis. Overall, the sediment texture and distribution patterns support a depositional environment marked by reworking and sorting processes favorable for the enrichment of phosphate minerals.

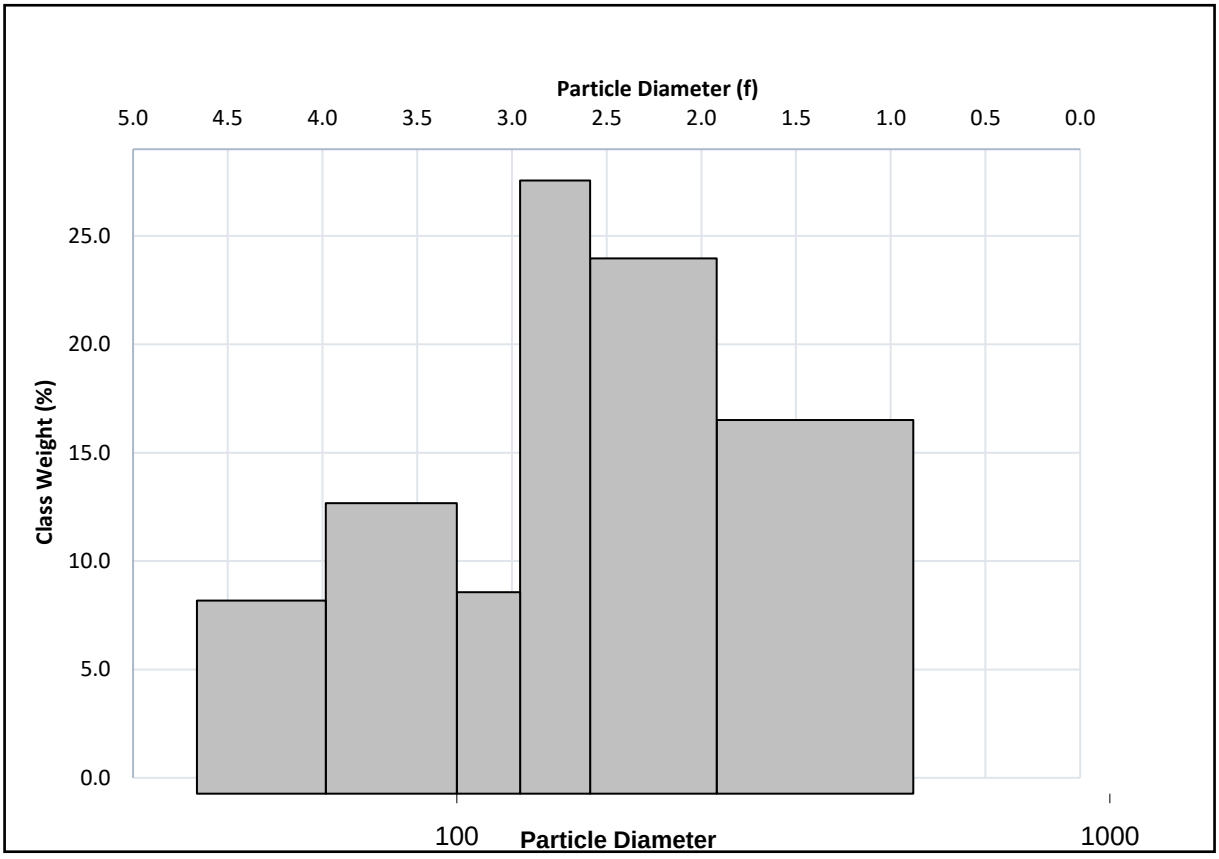

Fig.33: Grain size distribution of Upper Layer.

Fig.34: Distribution (microns) of Upper Layer.

Fig.35: Cumulative (microns) of Upper Layer.

Conclusion

The petrographic, mineralogical, and grain size analyses conducted on the phosphate samples from the Tarfaya deposit reveal a predominantly fine sand texture composed mainly of coprolites, pellets, glauconite, and minor bioclasts. Mineralogically, the samples are characterized by a dominance of carbonate fluorapatite (CFA), with accessory minerals such as quartz and dolomite. grain size data suggest moderate to poor sorting and generally symmetrical distributions. These findings highlight the dynamic sedimentary conditions and complex diagenetic processes that have influenced phosphate formation in this region, contributing valuable information for both academic research and resource exploitation.

CHAPTER IV
GEOCHEMICAL

CHAPTER IV

GEOCHEMICAL

Introduction

This chapter provides a comprehensive overview of the geochemical methodologies applied in the analysis of phosphate samples, with a particular focus on the physicochemical techniques used in the determination of major constituents such as P_2O_5, MgO, and CO_2. The focus is on sample preparation and processing using different acid attacks-perchloric, nitro-hydrochloric, nitro-hydrochloric, and sulfonitric-each designed for specific analytical applications such as spectrophotometry and gravimetry. Analytical techniques, including automated P_2O_5 photoluminescence spectrometry, magnesium oxide atomic spectrometry, and Bernard CO_2 measurement, are thoroughly described in terms of principles, reagents, operating procedures, and instrumentation conditions. In addition, statistical evaluation of oxide concentrations across multiple samples (from Ta2 to Ta7) provides insight into elemental variation and geochemical correlations within the studied phosphate matrix.

1. Physico-chemical analyses

1.1. Perchloric attack

Analysis of natural phosphates in the chemistry laboratory is mainly carried out using three methods of attack, depending on the analytical technique employed:

- **Perchloric attack:** for spectrophotometric methods
- **Nitro-hydrochloric attack:** alternative for spectrophotometric methods
- **Sulfonitric attack:** for gravimetric P_2O_5 method

1.1.1. Method

Hot solutionization of rock phosphate samples $Ca_3(PO_4)_2$ by attack with concentrated perchloric acid $HClO_4$, allowing complete phosphate solubilization for subsequent analysis.

- **Chemical reaction:**

$$Ca_3(PO_4)_2 + 2\ HClO_4 \rightarrow Ca(ClO_4)_2 + 2\ CaHPO_4$$

- **Ionic equation :**

$$3\ Ca^{2+} + 2\ PO_4^{3-} + 2\ H^+ + 2\ ClO_4^- \rightarrow Ca^{2+} + 2\ ClO_4^- + 2\ Ca^{2+} + 2\ HPO_4^{2-}$$

1.1.2. Reagents

- Pure perchloric acid for analysis (d = 1.62; 70% by weight)
- Distilled water

1.1.3. Operating mode

- **Sample preparation:**

- Accurately weigh 1,000 g of finely ground sample (< 100 mesh);
- Place in a 250 mL beaker;

- **Acid digestion:**

- Add a few mL of distilled water to moisten the sample;
- Slowly add 15 mL of concentrated perchloric acid;
- Heat in a sand bath at moderate temperature (150-200°C);
- Continue heating until complete disappearance of white coloration;

- **Digestion:**

- Let cool to room temperature;
- Transfer quantitatively into a 500 mL volumetric flask;
- Rinse the beaker thoroughly with distilled water;
- Adjust to the gauge and homogenize;

- **Filtration:**

- Filter through pleated filter paper;
- Discard the first few mL of filtrate;
- Collect filtrate in a dry, labeled bottle.

1.2. Dosage of P_2O_5 by Automatic Spectrophotometry

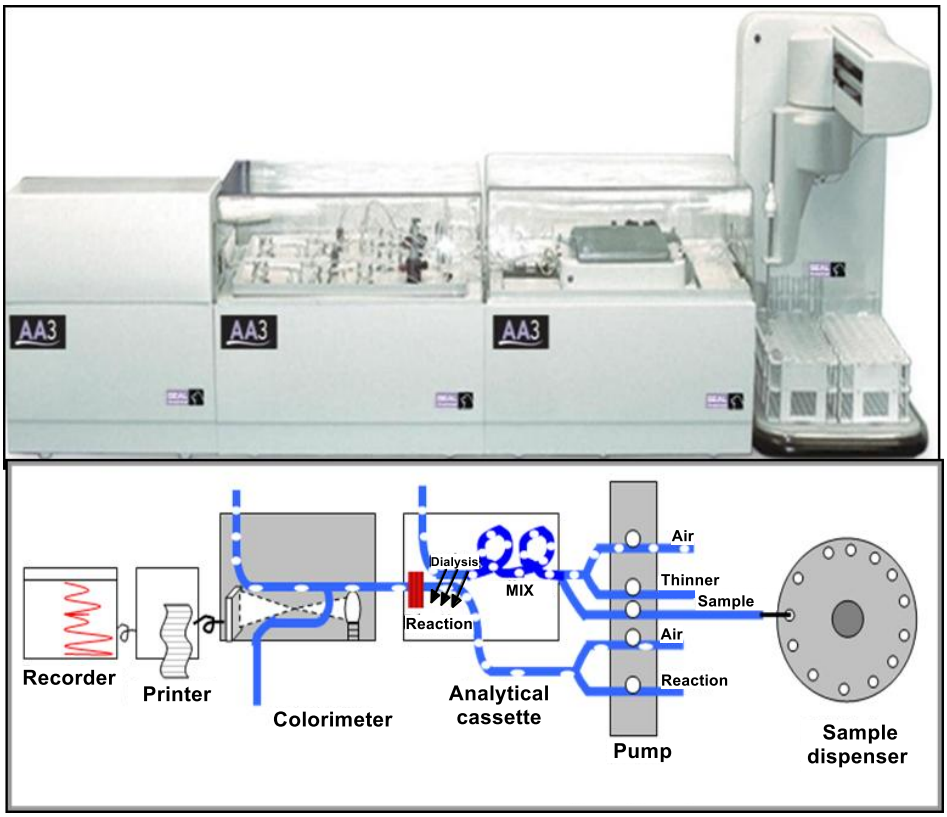

Fig.36: AA3 HR AutoAnalyzer (Legacy System).

1.2.1. Method

Formation of a yellow complex between phosphoric ions and vanadic-molybdic reagents, followed by automatic spectrophotometric determination at $\lambda = 430$ nm.

1.2.2. Instrumentation

- **Technicon autoanalyzer:**

- Speed: up to 120 samples/hour.
- Modular system with proportioning peristaltic pump.
- Integrated colorimeter with 430 nm filter.
- Graphic recorder for data acquisition.

1.2.3. Reagents

- **Acids**:

- Nitric acid HNO_3 (d = 1.38; 65% by weight).
- Perchloric acid $HClO_4$ (d = 1.61; 70% by weight).

- **Vanado-molybdic reagent:**

- **Solution A:** Mix 1 volume of concentrated nitric acid with 2 volumes of distilled water (2000 mL total).

Solution B:

- Dissolve 5.0 g of ammonium metavanadate (NH_4VO_3) in 500 mL of boiling distilled water.
- Add 40 mL of concentrated nitric acid.
- Complete to 2000 mL after cooling.

Solution C:

- Dissolve 100 g ammonium molybdate ($Mo_7O_{24}(NH_4)_6$-$4H_2O$) in 1500 mL boiling water.
- Complete to 2000 mL with hot distilled water.

Mix the three solutions in equal proportions (1:1:1) at the time of use.

1.2.4. Preparation of Standard Solutions

- **Mother solution (10 mg/mL as P_2O_5):**

- Dry KH_2PO_4 at 105°C for 2 hours.
- Weigh 19.174 g of dried KH_2PO_4.
- Dissolve in a 1000 mL volumetric flask.

- **Daughter standard solution :**

- Prepare 7 solutions in 500 mL flasks.
- Take 0, 5, 10, 15, 20, 25, 30 mL mother solution respectively.
- Add 15 mL of nitric acid to each flask.
- Complete to volume with distilled water.
- Final concentrations: 0, 5, 10, 15, 20, 25, 30% P_2O_5

1.2.5. Apparatus

- Technicon autoanalyzer with specific P_2O_5 manifold.
- 430 nm interference filter.
- Standard laboratory materials.

1.3. Dosage of magnesium (MgO) by atomic absorption

1.3.1. Method

Quantitative determination of magnesium by atomic absorption spectrometry in the presence of lanthanum oxide as a spectrochemical buffer to eliminate interferences.

1.3.2. Reagents

- **Concentrated hydrochloric acid** (d = 1.19; 37% by weight)
- **Mother standard solution:** 1000 mg/L magnesium
- **Daughter standard solution**: 100 mg/L magnesium (1:10 dilution)
- **Lanthanum spectrochemical buffer:**

- Weigh 58.64 g of La_2O_3
- Carefully dissolve in 250 mL of concentrated HCl
- Complete to 1000 mL in a volumetric flask.

1.3.3. Calibration range

In a series of 100 mL flasks, introduce successively:

- Volumes of daughter solution: 0.5, 1, 2, 4, 6 mL
- Lanthanum buffer: 2 mL in each vial
- Concentrated HCl: 2 mL in each vial.
- Add distilled water to the gauge line.

Final concentrations: 0.5, 1, 2, 4, 6 mg/L in magnesium

1.3.4. Operating conditions

- **Wavelength:** 285.2 nm
- **Flame:** Air-acetylene
- **Lamp:** Hollow magnesium cathode
- **Test sample:** 5 mL perchloric etching solution diluted to 100 mL

1.3.5. Apparatus

- Atomic absorption spectrophotometer (model AAS3300).
- Magnesium hollow cathode lamp.
- Air-acetylene burner.
- Compressed air and acetylene system.

1.4. Determination of carbon dioxide (CO_2) by Bernard Calcimetry

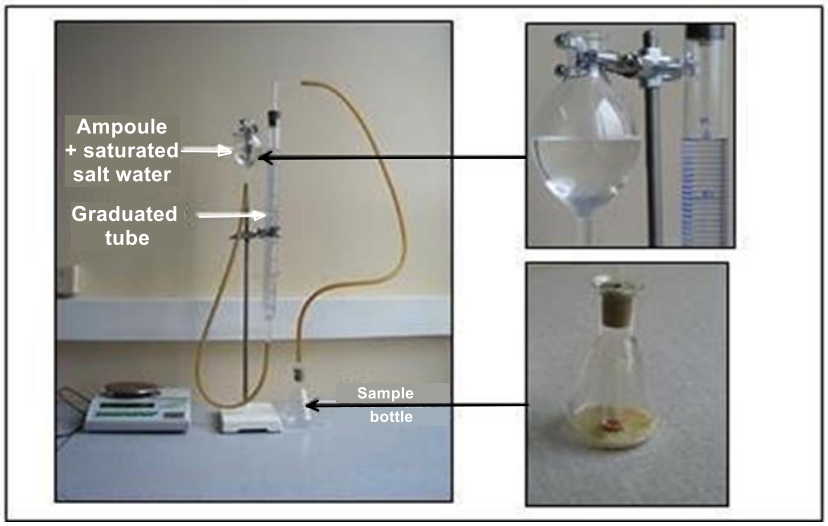

Fig.37: Method determination of carbon dioxide (CO_2) by Bernard Calcimetry

1.4.1. Method

Volumetric measurement of the CO_2 released by the action of hydrochloric acid on the carbonates present in the sample in a closed recipient at constant temperature.

1.4.2. Reaction

$CaCO_3 + 2\ HCl \rightarrow CaCl_2 + H_2O + CO_2\uparrow$

1.4.3. Reagents

- **Hydrochloric acid:** 50% solution by volume.
- Anhydrous copper sulfate: to prevent the release of H_2S.
- Standard: pure, dry calcium carbonate.

1.4.4. Apparatus

Bernard calcimeter comprising:

- Pear flask with side tube.
- Graduated measuring tube.
- Variable-level reservoir.
- Thermometer.
- Glass beads (agitation).

1.4.5. Operating mode

- **Preparation**

- Weigh 1,000 g of ground sample into the dry Pear flask.
- Place 10-12 glass beads in the flask.
- Add 5 mL of 50% HCl to a hemolysis tube.
- Place the tube in the flask without inverting the liquid.

- **Reaction and measurement**

- Incline flask to mix acid and sample.
- Equilibrate liquid levels in the measuring tube and reservoir.
- Stir continuously until the level stabilizes.
- Leave to cool without stirring.

- **Reading**

- Record temperature and volume every 5 minutes.
- Take a final reading at the initial temperature.
- Keep levels balanced in both branches.

2. Results and interpretations

2.1. Vertical Geochemical Trends of Major Components

The concentrations of P_2O_5, MgO, and CO_2 exhibit clear stratigraphic differentiation across the basal, main, and upper layers of the phosphate succession, reflecting variations in depositional and post-depositional processes (Table 5).

2.1.1. Basal Layer

This layer shows moderate phosphate content, with P_2O_5 values ranging from 22.13% to 24.52% (average: 23.33%). The MgO content is relatively low, averaging 1.99%, with minimal values (0.84%) indicative of limited dolomitic or magnesian influence. The CO_2 content varies from 5.31% to 11.63% (average: 8.47%), reflecting the presence of carbonate phases, possibly linked to bioclastic or micritic components. The relatively low standard deviation in P_2O_5 (1.69%) suggests chemical homogeneity in phosphate enrichment at the base.

2.1.2. Main Layer

This unit exhibits the widest compositional variability. P_2O_5 content ranges from 19.61% to 31.07% (average: 27.18%), with a high standard deviation (6.56%) suggesting heterogeneous phosphate accumulation. The MgO content also fluctuates significantly (0.76%–3.79%, avg. 1.77%), possibly due to variations in dolomitic input or detrital contamination. CO_2 concentrations are highest in this layer (up to 14.11%), indicating substantial carbonate content, which may reflect enhanced biogenic or diagenetic processes.

2.1.3. Upper Layer

Represented by sample Ta07, this level shows intermediate P_2O_5 (26.19%) and elevated MgO (2.66%), alongside a moderate CO_2 value (8.97%). These values suggest a transitional composition, potentially reflecting residual enrichment or mixing between phosphate-rich and carbonate-rich facies.

Table 5: Table of summary of P_2O_5, MgO, and CO_2 Concentrations in Samples Ta2–Ta7 with Statistical Parameters.

		P_2O_5	**MgO**	**CO_2**
Basal layer	**Ta02**	22.13	0.84	5.31
	Ta03	24.52	3.13	11.63
	MIN	22.13	0.84	5.31
	MAX	24.52	3.13	11.63
	AVERAGE	23.33	1.99	8.47
	STDEV	1.69	1.62	4.47
Main layer	**Ta04**	31.07	0.77	5.97
	Ta05	30.86	0.76	4.32
	Ta06	19.61	3.79	14.11
	MIN	19.61	0.76	4.32
	MAX	31.07	3.79	14.11
	AVERAGE	27.18	1.77	8.13
	STDEV	6.56	1.75	5.24
Upper layer	**Ta07**	26.19	2.66	8.97

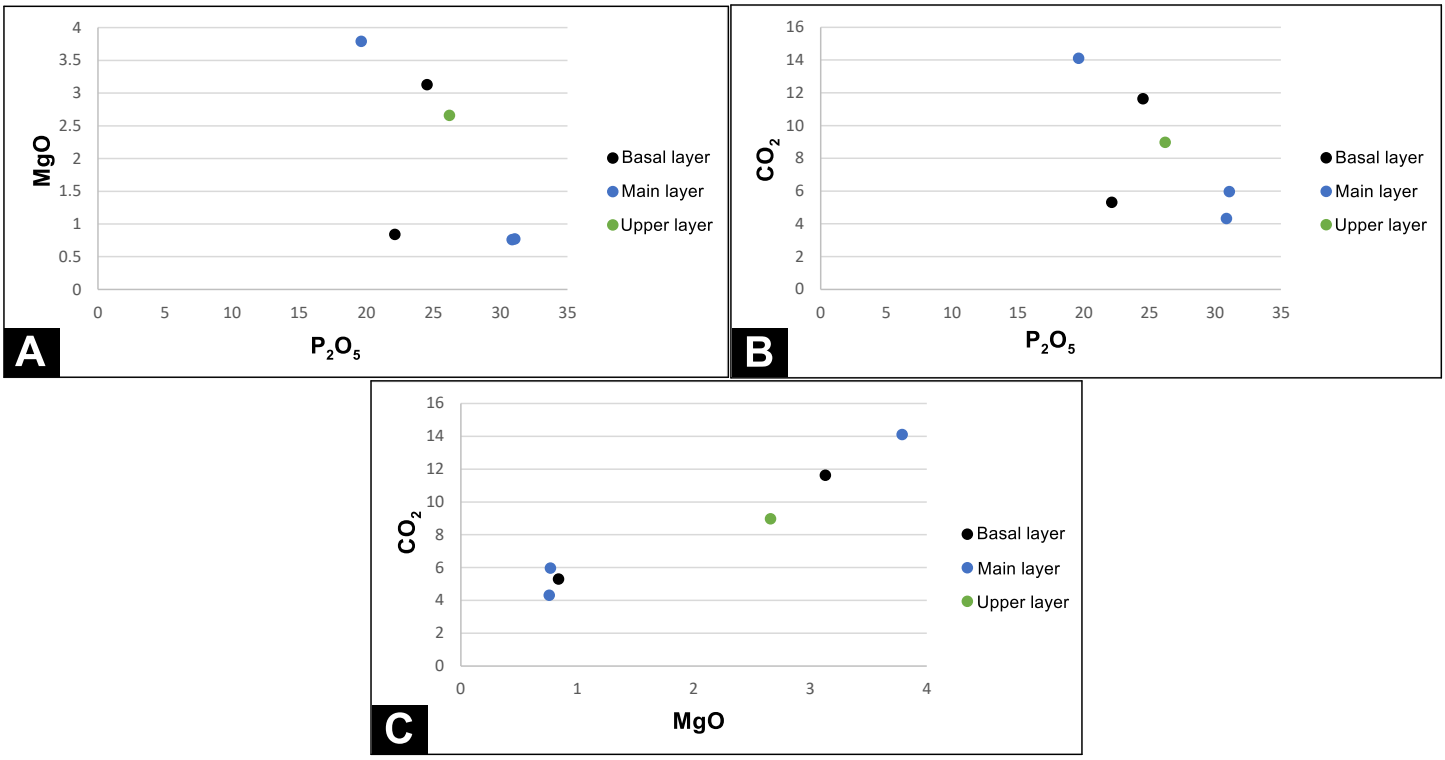

Fig.38: Geochemical relationships between P_2O_5, MgO, and CO_2.

A: P_2O_5 vs. MgO: shows an inverse or weakly scattered relationship. / **B:** P_2O_5 vs. CO_2: shows a clear inverse correlation. / **C:** MgO vs. CO_2: shows a positive correlation.

2.2. Correlation Analysis of Major Components

The correlation matrix reveals significant interrelationships among the major chemical components (P_2O_5, MgO, and CO_2) in the phosphate-bearing samples (Table 6):

- **P_2O_5 is negatively correlated** with both **MgO (r = -0.66)** and **CO_2 (r = -0.68)**, indicating that higher phosphate contents tend to be associated with lower concentrations of magnesian and carbonate phases. This inverse relationship may reflect competitive mineralogical associations, where phosphate minerals (e.g., apatite) are spatially or diagenetically distinct from dolomite or carbonate-rich components (Fig. 44.A&B).
- **MgO and CO_2 exhibit a strong positive correlation (r = 0.98)**, suggesting that these two elements are co-associated, likely reflecting the contribution of **dolomitic carbonates**, where Mg and CO_3 are structurally bound. This co-variation reinforces the interpretation of **dolomite or mixed carbonate inputs** in layers with elevated MgO and CO_2 (Fig. 44.C).
- The negative correlations of **P_2O_5 with both MgO and CO_2** may also imply **lithological differentiation**, with phosphate-rich facies being relatively depleted in dolomitic or carbonate material, and vice versa.

- **Table 6:** Correlation matrix of chemical elements (oxides) in phosphate ores from the Tarfaya region.

Variables	**P_2O_5**	**MgO**	**CO_2**
P_2O_5	1		
MgO	-0.66	1	
CO_2	-0.68	0.98	1

2.3. Interpretation

The observed stratigraphic variation in P_2O_5, MgO, and CO_2 concentrations reflects distinct depositional and diagenetic processes shaping the phosphate succession. The basal layer's chemical homogeneity and moderate phosphate content suggest deposition under stable, low-energy marine conditions with balanced carbonate input. In contrast, the main layer's compositional variability indicates dynamic sedimentation, with fluctuating phosphate input and episodic carbonate or dolomite influx, possibly driven by changes in sea level, sediment sources, or biological productivity. The transitional nature of the upper layer points to a shift towards mixed facies, reflecting either waning phosphate accumulation or increased detrital/carbonate influence. The strong negative correlation between P_2O_5 and both MgO and CO_2 highlights mineralogical segregation, where phosphate-rich sediments are relatively depleted in dolomitic carbonates, supporting the interpretation of facies differentiation and diagenetic overprinting within the sequence.

Conclusion

The geochemical study of phosphate samples from the Tarfaya region, conducted through rigorous Physico-chemical methods, provides valuable insights into the compositional variability and mineralogical characteristics of the deposit's stratigraphic layers. The application of targeted acid attack procedures, coupled with advanced spectrophotometric and atomic absorption techniques, enabled precise quantification of key constituents such as P_2O_5, MgO, and CO_2.

The results revealed a distinct geochemical stratification. The basal layer contains moderate levels of apatite and a variably dolomitic matrix. The main layer is marked by high

heterogeneity, ranging from apatite-rich to dolomite-dominant zones, reflecting significant lithological diversity. The upper layer demonstrates intermediate characteristics, suggesting a transitional zone between apatite and dolomite mineralization.

Correlative analysis highlighted an inverse relationship between P_2O_5 and both MgO and CO_2, underscoring the competitive nature of apatite and dolomite deposition within the geological environment. The strong positive correlation between MgO and CO_2 confirms the dolomitic origin of these constituents. Collectively, these findings contribute to a better understanding of the depositional and diagenetic processes shaping the phosphate-bearing formations of the region and support further exploration and improvement efforts.

GENERAL CONCLUSION

GENERAL CONCLUSION

The phosphate resources of the Tarfaya region, located in the southern part of the Djebel Onk mining basin, represent one of the most significant sedimentary phosphate accumulations in Algeria. This dissertation has focused on the geological, mineralogical, grain size, and geochemical characterization of these deposits, particularly through the study of the Kef Essenoun-Tarfaya zone. The aim was to assess the nature of the phosphate-bearing layers and understand the processes that influenced their formation and evolution. The following summarizes the key findings:

Petrologically:

Petrographic analysis of the Tarfaya phosphorite succession reveals a consistent composition dominated by coprolites and pellets (≈50%), with variable contents of glauconite (1–5%), carbonate cement (43–48%), and minor fish teeth (1%), across the basal, main, and upper sub-layers. Microscopic observations confirm that coprolites and pellets are the primary phosphate constituents, differing in shape, porosity, and origin. Glauconite occurs intergranularly and increases slightly upwards in the sequence, reflecting evolving depositional and early diagenetic conditions. These features indicate moderate sedimentary reworking and early mineral transformations consistent with phosphogenic environments.

Mineralogy:

XRD analysis confirms that carbonate fluorapatite (CFA) is the dominant mineral phase in the studied phosphate sample, with characteristic peaks at 3.488 Å, 2.935 Å, 2.709 Å, and 2.232 Å, typical of sedimentary phosphorites. Quartz and dolomite are present as major accessory minerals, identified by distinct peaks, while hulsite(?) appears in trace amounts with tentative assignments. The analysis of the <45 μm fraction enhanced the detection of these phases. These mineralogical associations align with patterns observed in regional Algerian-Tunisian phosphate deposits.

Grain Size:

Grain size analysis of sedimentary phosphates from the Tarfaya deposit (Djebel Onk, southern Tébessa) reveals a dominance of fine to medium particles, low clay content (<2%), and generally well to moderately sorted sediments (0.57–1.08 Φ). Median sizes range from 2.25 to 2.75 Φ, with near-symmetrical to slightly skewed (–0.12 to +0.30) and mesokurtic to platykurtic

(0.85–1.25) distributions, indicating stable depositional conditions. Most layers display homogeneous, monomodal grain-size curves, suggesting reworking and hydrodynamic sorting, while basal layers show more heterogeneity and finer fractions, reflecting fluctuating energy conditions. These features support a model combining primary phosphate precipitation with secondary reworking on a shallow marine platform.

Geochemically:

The geochemical composition of the phosphate succession reveals distinct stratigraphic differentiation driven by depositional and diagenetic processes. The basal layer shows moderate and homogeneous phosphate enrichment (P_2O_5 avg. 23.33%, MgO 1.99%, CO_2 8.47%), indicating limited dolomitic and carbonate influence. The main layer is more heterogeneous, with P_2O_5 ranging from 19.61% to 31.07% (avg. 27.18%), higher CO_2 (up to 14.11%), and variable MgO (0.76–3.79%), reflecting mixed inputs and diagenetic alteration. The upper layer (Ta07) presents intermediate P_2O_5 (26.19%), elevated MgO (2.66%), and moderate CO_2 (8.97%), suggesting transitional facies.

Correlation analysis shows that P_2O_5 is negatively correlated with MgO ($r = -0.66$) and CO_2 ($r = -0.68$), while MgO and CO_2 are strongly positively correlated ($r = 0.98$), highlighting mineralogical contrasts between phosphate-rich and carbonate-rich layers. These trends emphasize the role of depositional conditions and post-depositional processes in controlling phosphate and carbonate distribution.

REFERENCES

REFERENCES

Aissaoui, D. (1984). Les structures liées al'accident sud-atlasique entre Biskra et le Djebel Manndra, Algérie. Évolution géométrique et cinématique. These 3eme cycle, Strasbourg, 138.

Aly, M. M., & Mohammed, N. A. (1999). Recovery of lanthanides from Abu Tartur phosphate rock, Egypt. *Hydrometallurgy*, *52*(2), 199-206.

Baioumy, H. M. (2005). Preliminary data on cadmium and arsenic geochemistry for some phosphorites in Egypt. Journal of African Earth Sciences, 41(3), 266-274.

Baturin, G.N. (1982). Phosphorite on the sea floor: origin, composition and distribution. In: Developments in Sedimentology Elsevier, 33, 355.

Baturin, G. N., & Kochenov, A. V. (2001). Uranium in phosphorites. Lithology and mineral resources, 36, 303-321.

Béji-Sassi, A. (1999). Les phosphates dans les bassins paléogènes de la partie méridionale de l'Axe Nord-Sud (Tunisie). *Thèse Doct.* d'État, *Université Tunis II, Tunisie*.

Ben Hassen, A., Trichet, J., Disnar, J.-R., Belayouni, H. (2010). Petrographie et geochimie comparees des pellets phosphat es et de leur gangue dans le gisement phosphate de Ras-Draa (Tunisie). Implications Sur la genèse des pellets phosphates. Swiss J. Geosci. 103, 457–473.

Bezzi, N., Aïfa, T., Hamoudi, S., Merabet, D. (2012). Trace elements of Kef Es sennoun natural Phosphate (Djebel Onk, Algeria) and how they affect the various Mineralurgic modes of treatment. Procedia Engineering 42: 1915–1927. https://doi.org/10.1016/j.proeng.2012.07.588

Burnett, W.C., Glenn, C.R., & Föllmi, K.B. (1990). Phosphorite research and development. In: Burnett, W.C., & Riggs, S.R. (Eds.), Phosphorite Research and Development (pp. 1–11). Geological Society of America Special Paper 228.

Chaabani, F. (1995). Dynamique de la partie orientale du bassin de Gafsa au Crétacé et au Paléogène : Etude minéralogique et géochimique de la série phosphatée Eocène, Tunisie méridionale. Thèse Doct. Etat, Univ. Tunis II, Tunisie.

Chabou-Mostfai, S. (1975). Projet de recherche de la minéralisation phosphatée à l'est du méridien d'Alger, en Algérie. *Algérie: Rapport SONAREM (Société Nationale Algérienne de Recherche et d'Exploration Minière)*.

Chabou-Mostefai. (1987). Etude de la série stratigraphique tertiaire du Djebel Onk (Algérie). Leur situation dans le cadre des phosphates algériens. DEA, Fac. Sci. Alger, 136p.

Cherniak, D.J. **(2000).** Rare earth element diffusion in apatite. *Geochimica et Cosmochimica Acta*, 64(3),387–398.https://doi.org/10.1016/S0016-7037(99)00333-0:contentReference[oaicite:4]{index=4}

Cielensky, S., Benchernine, N. (1987). Travaux de prospection et d'évaluation des phosphates dans la région de Bir El Ater. Rapport interne, EREM, 80p

Cielensky, S., Benchernine, N., & Watkowski, T. (1988). Works of prospecting and assessment of phosphates in the region of Bir El Ater. In *Internal Report. 2* (p. 103). EREM (Entreprise de Recherche et d'Exploration Minière) Algeria.

Cissé, L., Mrabet, T. (2004). World Phosphate Production: Overview and Prospects. Phosphorus Res. Bull. 15, 21–25.

Cook, P.J. (1986). Phosphogenesis around the world: Implications for understanding the deposition of phosphorites. In: Cook, P.J., & Shergold, J.H. (Eds.), Phosphate Deposits of the World, Vol. 1: Proterozoic and Cambrian phosphorites (pp. 3–32). Cambridge University Press.

El Bamiki, R., Raji, O., Ouabid, M., Elghali, A., Khadiri Yazami, O., & Bodinier, J. L. (2021). Phosphate rocks: A review of sedimentary and igneous occurrences in Morocco. *Minerals*, *11*(10), 1137.

EREM. (1987). Travaux de Prospection et d'Evaluation des Phosphates dans la région de Bir

El Ater, Tome 1 : Géologie, Tome 2 : Prospection- Evaluation

Ferhaoui. S, 2023. Les minéralisations phosphatées du gisement de Kef Essenoun-Djebel Onk (Algérie Orientale) : chimiostratigraphie et implications sur la reconstruction paléo-environnementale.

Fisher, A.G., Jérom, D. (1973). Geochimistry of minerals containing phosphorus, in Environmental Phosphorus Handbook, 141p – John Wiley and Sons. New-York, London, Sydney, Toronto.

Filippelli, G.M. (2011). Phosphate rock formation and marine phosphorus geochemistry: The deep time perspective. Chemical Geology, 282(3–4), 282–290. https://doi.org/10.1016/j.chemgeo.2010.08.017

Föllmi, K.B. (1996). The phosphorus cycle, phosphogenesis and marine phosphate-rich deposits. Earth-Science Rev. 40, 55–124.

Föllmi, K.B. (2016). Sedimentary condensation. Earth-Science Rev., 152, 143–180.

Föllmi, K.B., Garrison, R.E., & Wright, V.P. (1993). Phosphorite deposition on the Neocomian Urgonian platform of the Helvetic Alps (eastern Switzerland): a model for phosphogenesis in shallow carbonate environments. Sedimentology, 40(3), 567–589.

Folk, R. L., & Ward, W. C. (1957). Brazos River bar: A study in the significance of grain size parameters. Journal of Sedimentary Petrology, 27(1), 3–26.

Funk, H., Föllmi, K. B., & Mohr, H. (1993). Evolution of the Tithonian–Aptian carbonate platform along the northern Tethyan margin, eastern Helvetic Alps.

Galfati, I., Sassi, A.B., Zaier, A., Bouchardon, J.L., Bilal, E., Joron, J.L., Sassi, S. (2010). Geochemistry and mineralogy of Paleocene-Eocene Oum El Khecheb phosphorites (Gafsa-Metlaoui Basin) Tunisia. Geochem. J. 44 (3), 189–210.

Garnit, H., Bouhlel, S., Jarvis, I. (2017). Geochemistry and depositional environments of Paleocene-Eocene phosphorites: Metlaoui Group, Tunisia. J. Afr. Earth Sci. 134, 704–736. https://doi.org/10.1016/j.jafrearsci.2017.07.021.

Glenn, R.C., Follmi, K.B., Riggs, S.R., Baturin, G.N., Grimm, K.A., Trappe. J., Abed, A.M., Galli-Olivier, C., Garrison, R.E., Ilyin, A., Jehl, C., Roharlich, V., Sadaqah, R.M., Schidlowski, M., Sheldon, R.E., Siegmund, H. (1994). Phosphorus and phosphorites: sedimentology and environments of formation. Eclogae Geol Helv 87: 747–788.

Jasinski, S.M. (2020). Mineral commodity summaries: Phosphate Rock. U.S. Geol. Surv. 705, 122–123.

Jarvis, I., Burnett, W.C., Nathan, Y., Almbaydin, F.S.M., Attia, A.K.M., Castro, .LN., Flicoteaux, R., Hilmy, M.E., Husain, V., Qutawnah, A.A., Serjani, A., Zanin, Y.N. (1994). Phosphorite geochemistry—state-of-the-art and environmental concerns. Eclogae Geologicae Helvetiae (Journal of the Swiss Geological Society) 87: 643–700

Kechiched, R., Laouar, R., Bruguier, O., Salmi-Laouar, S., Ameur-Zaimeche, O., Foufou, A. (2016). Preliminary Data of REE in Algerian Phosphorites: A Comparative Study and Paleo-redox Insights. *Procedia Engineering*, 138, 19–29. https://doi.org/10.1016/j.proeng.2016.02.048

Kechiched, R. (2017). Les phosphates du Nord de Tébessa : Etude sedimentologique, gîtologique et geochimique. These doctorat en sciences, Université Badji Mokhtar Annaba. 184 p.

Kechiched, R., Laouar, R., Bruguier, O., Salmi-Laouar, S., Kocsis, L., Bosch, D., ... & Larit, H. (2018). Glauconite-bearing sedimentary phosphorites from the Tébessa region (eastern Algeria):

Evidence of REE enrichment and geochemical constraints on their origin. *Journal of African Earth Sciences, 145*, 190-200.

Kechiched, R., Laouar, R., Bruguier, O., Kocsis, L., Salmi-Laouar, S., Bosch, D., Ameur-Zaimeche, O., Foufou, A., Larit, H. (2020). Comprehensive REE + Y and sensitive redox trace elements of Algerian phosphorites (Tebessa, eastern Algeria): a geochemical study and depositional environments tracking. Journal of Geochemical Exploration, *208*, 106396. https://doi.org/10.1016/j.gexplo.2019.106396.

Krajewski, K.P., Van Cappellen, P., Trichet, J., Kuhn, O., Lucas, J., Dedeckker, P., Glenn, C.R., & Filippelli, G.M. **(1994).** Biological processes and apatite formation in sedimentary environments. Eclogae Geologicae Helvetiae, 87, 701–745.

Larouci, M. (1988). Study of the characterization and the valorization of phosphate ore of Djebel Onk, Algeria (Doctoral thesis, Ph. D. Thesis, University of Orleans, France).

Lamboy, M., Rao, V.P., Ahmed, E., Azzouzi, N. (1994). Nannostructure and significance of fish coprolites in phosphorites. Marine Geology 120: 373-383.

McClellan G.H, Lchr J.R. (1969). Crystal chemical investigation of natural apatite. Am. Mineral. 54, pp. 1375-1391.

Mezghache, H., Hani, A. (2000). Typologie chimique des phosphates du gisement de Djemi-Djema-bassin de Djebel Onk (Algérie orientale). Géologie Méditerranéenne, 27(1), 95-106.

Northolt, M. D., Van Egmond, H. P., Soentoro, P., & Deijll, E. (1980). Fungal growth and the presence of sterigmatocystin in hard cheese. *Journal of the Association of Official Analytical Chemists*, *63*(1), 115-119.

Ounis, A., Kocsis, L., Chaabani, F., Pfeifer H.R. (2008). Rare earth elements and stable isotope geochemistry ($\delta^{13}C$ and $\delta^{18}O$) of phosphorite deposits in the Gafsa Basin, Tunisia. Palaeogeography, Palaeoclimatology, Palaeoecology 268 : 1–18. https://doi.org/10.1016/j.palaeo.2008.07.005

Prian, G.P., Cortiel, Ph. (1993). In : Etude de developpement du gisement de phosphate de Djebel Onk (Algerie), Rapport d'expertise geologique. B.R.G.M, France, p. 288.

Pufahl, P.K., Groat, L.A. (2017). Sedimentary and igneous phosphate deposits: Formation and exploration: An invited paper., 112, 483–516.

Pufahl, P.K., Grimm, K.A., Abed, A.M. and Sadaqah, R.M.Y. (2003). Upper Cretaceous (Campanian) phosphorites in Jordan: Implications for the formation of a south Tethyan phosphorite giant. Sediment. Geol. 161, 175–205.

Rakovan, J., & Reeder, R. J. (1996). Intracrystalline rare earth element distributions in apatite: Surface structural influences on incorporation during growth. Geochimica et Cosmochimica Acta, *60*(22), 4435-4445.

Ranchin, G. (1963). Les phosphates de chaux sédimentaire de la région du Djebel Onk (Algérie), S.E.R.M. Paris, p 85.

Saïd, A., Baby, P., Chardon, D.,Ouali, J. (2011). Structure, paleogeographic inheritance, and deformation history of the southern Atlas foreland fold and thrust belt of Tunisia. Tectonics, 30(6).

Sassi, S., 1974. La sedimentation phosphatee au Paleocene dans le Sud et le Centre Ouest de la Tunisie. Univ. de Paris Sud. These de Doct. d'etat es Sci.

Sassi, G. (1980). Chromatic dispersion concentrator applied to photovoltaic systems. Solar Energy, 24(5), 451-460.

Sengul, H., Ozer, A. K., Gulaboglu, M. S. (2006). Beneficiation of Mardin-Mazıdağı (Turkey) calcareous phosphate rock using dilute acetic acid solutions. Chemical Engineering Journal, 122(3), 135-140.

Simon. J Blott. (2010) : Gradistat. v8.0.grain programme d'analyse granulométrique.

Slansky, M. (1980). Géologie des phosphates sédimentaires, Mem. Du BRGM. No.114-1980, 3 p.

Soudry, D., Nathan, Y. and Ehrlich, S. (2013). Geochemical diagenetic trends during phosphorites formation - economic implications: The case of the Negev Campanian phosphorites, Southern Israel. Sedimentology, 60, 800–819.

Trappe, J. (1998). Phanerozoic Phosphorite Depositional Systems": a Dynamic Model for a Sedimentary Resource System. Springer Berlin Heidelberg. 316 pp.

USGS - U.S. Geological Survey. (2020). Mineral Commodity Summaries 2020: U.S. Geological Survey, 200 p. https://doi.org/10.3133/mcs2020 (Accessed date: 11/12/ 2021).

Visse, L. (1951). Le gisement de phosphate de chaux de Djebel Onk. Rapport interne Soc. Dj. Onk.

Visse, L. (1952). Genèse des gîtes phosphatés du Sud-est Algéro–tunisien, XIX Congrès géol Intern Alger, série 1, no 27, p 60.

Wikimedia commons. (https://commons.m.wikimedia.org/w/index.php#/search).

Zaïer, A., Béji-Sassi, A., Sassi, S., Moody, R.T.J. (1998). Basin evolution and deposition during the early Paleocene in Tunisia. In: Macgregor DS, Moody RTJ, Clark-Lowes DD (Eds) Petroleum Geology of North Africa. Geological Society, London, Special Publications, pp 375–393

Zargouni, F. (1985). Tectonique de l'Atlas méridional de Tunisie, évolution géométrique et cinématique des structures en zone de cisaillement. Thèse d'Etat, Univ Louis Pasteur, Strasbourg-Paris

Zhang, L., Wang, Y., Miao, X., Gan, M.,Li, X. (2019). Geochemistry in geologic CO2 utilization and storage: A brief review. Advances in Geo-Energy Research, 3(3), 304-313.